Unclassified
SECURITY CLASSIFICATION OF THIS PAGE (When Data Entered)

REPORT DOCUMENTATION PAGE		READ INSTRUCTIONS BEFORE COMPLETING FORM
1. REPORT NUMBER N00014-80-C-0838-AR4	2. GOVT ACCESSION NO.	3. RECIPIENT'S CATALOG NUMBER
4. TITLE (and Subtitle) Research on Acoustical and Optical Scattering, Optics of Bubbles, Diffraction Catastrophes, Laser Generation of Sound, and Shock Induced Cavitation		5. TYPE OF REPORT & PERIOD COVERED Annual Summary Report 1 July 83 - Sept. 84 6. PERFORMING ORG. REPORT NUMBER
7. AUTHOR(s) Philip L. Marston		8. CONTRACT OR GRANT NUMBER(s) N00014-80-C-0838
9. PERFORMING ORGANIZATION NAME AND ADDRESS Department of Physics Washington State University Pullman, WA 99164-2814		10. PROGRAM ELEMENT, PROJECT, TASK AREA & WORK UNIT NUMBERS Program Element: 61153N Task Area: RR011-08-01 Work Unit: NR384-934
11. CONTROLLING OFFICE NAME AND ADDRESS Physics Division Office (Code 412) Office of Naval Research Arlington, VA 22217		12. REPORT DATE September 1984 13. NUMBER OF PAGES 81
14. MONITORING AGENCY NAME & ADDRESS(if different from Controlling Office)		15. SECURITY CLASS. (of this report) Unclassified 15a. DECLASSIFICATION/DOWNGRADING SCHEDULE

16. DISTRIBUTION STATEMENT (of this Report)

Approved for public release; distribution unlimited

17. DISTRIBUTION STATEMENT (of the abstract entered in Block 20, if different from Report)

18. SUPPLEMENTARY NOTES

Research done in cooperation with: D. S. Langley, B. T. Unger, and K. L. Williams (current or former graduate students); and with J. H. Crichton and E. H. Trinh.

19. KEY WORDS (Continue on reverse side if necessary and identify by block number)

Acoustic scattering, Inverse scattering, Elastic-wave scattering, Backscattering, Sonar calibration, Physical acoustics, Underwater acoustics, Light scattering, Bubbles, Mie theory, Optical oceanography, Light extinction, Optoacoustics, Photoacoustics, Half-order derivative, Cavitation, Radiation Pressure, Catastrophe Optics, Diffraction Catastrophes, Rayleigh waves

20. ABSTRACT (Continue on reverse side if necessary and identify by block number)

The research summarized concerns a variety of phenomena associated with the propagation and scattering of acoustical, optical, and shock waves. The topics considered fall under the following four categories:

I. Acoustical scattering theory and experiments (focused backscattering from spheres due to transmitted wave and Rayleigh wave acoustical glories, nearfield effects in acoustic scattering, backscattering from a torus, and distortion of focused pulses);

20. Abstract (continued)

II. Scattering of light from bubbles in liquids and other problems in electromagnetic scattering of value to acoustics and naval technology (critical-angle scattering of light from bubbles, strong cross-polarization in near-forward and backward scattering from bubbles, optical measurement of the amplitude of radial oscillations of bubbles, an optical retro-reflector for use in water, a novel hyperbolic-umbilic diffraction catastrophe, and radiation torques on spheres);

III. Characterization of sound generated in water by modulated laser beams (production by a pre-existent bubble in water, radiation pressure, and heating in water); and

IV. Rapid cavitation induced by the reflection of shock waves.

DEPARTMENT OF PHYSICS

WASHINGTON STATE UNIVERSITY

PULLMAN, WA 99164-2814

REPORT NUMBER N00014-80-C-0838-AR4

ANNUAL SUMMARY REPORT NO. 4

SEPEMBER, 1984

RESEARCH ON ACOUSTICAL AND OPTICAL SCATTERING, OPTICS OF BUBBLES, DIFFRACTION CATASTROPHES, LASER GENERATION OF SOUND, AND SHOCK INDUCED CAVITATION

by

Philip L. Marston

Prepared for:

OFFICE OF NAVAL RESEARCH

CONTRACT NO. N00014-80-C-0838

TABLE OF CONTENTS

I. External Communications Supported by this Contract (since July 1, 1983)

A. Publications

1. P. L. Marston, K. L. Williams, and T. J. B. Hanson, "Observation of the acoustic glory: High-frequency backscattering from an elastic sphere," Journal of the Acoustical Society of America 74, 605-618 (1983).

2. P. L. Marston, J. L. Johnson, S. P. Love, and B. L. Brim, "Critical angle scattering of white light from a cylindrical bubble in glass: photographs of colors and computations," Journal of the Optical Society of America 73, 1658-1664 + Plate X (1983).

3. P. L. Marston, "Uniform Mie-theoretic analysis of polarized and cross-polarized optical glories," Journal of the Optical Society of America 73, 1816-1818 (1983).

4. D. S. Langley and P. L. Marston, "Critical-angle scattering of laser light from bubbles in water: Measurements, models, and applications to sizing of bubbles," Applied Optics 23, 1044-1054 (1984).

5. P. L. Marston, "Half-order derivative of a sine-wave burst: Applications to two-dimensional radiation, photoacoustics, and focused scattering from spheres and a torus," Journal of the Acoustical Society of America 76, 291-295 (1984).

6. P. L. Marston and J. H. Crichton, "Radiation torque on a sphere illuminated with circularly polarized light," Journal of the Optical Society of America B1, 528-529 (1984).

7. P. L. Marston and J. H. Crichton, "Radiation torque on a sphere caused by a circularly polarized electromagnetic wave," Physical Review A (accepted for publication).

8. K. L. Williams and P. L. Marston, "Mixed-mode acoustical glory scattering from a large elastic sphere: Model and experimental verification," Journal of the Acoustical Society of America (accepted for publication).

9. P. L. Marston and D. S. Langley, "Strong backscattering and cross-polarization from bubbles and glass spheres in water," Proceedings of the Society of Photo-Optical instrumentation Engineers, 489 (accepted for publication).

10. D. L. Langley and P. L. Marston, "Scattering of laser light from bubbles in water at angles from 68 to 85 degrees," Proceedings of the Society of Photo-Optical Instrumentation Engineers 489 (accepted for publication).

11. P. L. Marston and S. G. Goosby, "Ultrasonically stimulated low-frequency oscillation and breakup of immiscible liquid drops: Photographs," Physics of Fluids (submitted in 1984).

12. P. L. Marston and E. H. Trinh, "Rainbow scattering from spheroidal drops: a novel hyperbolic umbilic diffraction catastrophe," Nature (accepted for publication).

B. Papers presented at meetings or to be presented at meetings.

1. K. L. Williams and P. L. Marston, "Mixed-mode acoustic glory: Model and experimental verification," J. Acoust. Soc. Am. Suppl. 74, 109 (1983).

2. P. L. Marston and J. H. Crichton, "Radiation torque on a sphere illuminated with circularly polarized light," presented at the 13th International Quantum Electronics Conference (Anaheim, June 1984).

3. P. L. Marston and D. S. Langley, "Strong backscattering and cross-polarization from bubbles and glass spheres in water," Ocean Optics VII (Monterey, June 1984).
4. D. S. Langley and P. L. Marston, "Scattering of laser light from bubbles in water at angles from 68 to 85 degrees," Ocean Optics VII (Monterey, June 1984).
5. P. L. Marston and D. S. Langley, "Transmitted wave and rainbow-enhanced glories of dielectric spheres," presented at the 1984 Chemical Research and Development Center Scientific Conference on Obscuration and Aerosol Research (Aberdeen Proving Ground, MD, June 1984).
6. P. L. Marston and J. H. Crichton, "Radiation torque on a sphere illuminated with circularly polarized light," presented at the same CRDC Conference as the preceding item.

The following papers are to be presented at the 108th Meeting of the Acoustical Society of America (Minneapolis, October 1984):

7. K. L. Williams and P. L. Marston, "Axially-focused (glory) scattering due to surface waves on tungsten carbide spheres."
8. P. L. Marston and D. S. Langley, "Optical scattering properties of bubbles of interest in acoustics and cavitation research."
9. P. L. Marston and E. H. Trinh, "Light scattering from acoustically levitated spheroidal drops: Discovery of a new hyperbolic umbilic diffraction catastrophe."

C. Technical Reports issued under this Contract:

1. P. L. Marston, Technical Report No. 3. Focused Acoustical and Optical Backscattering from Spheres and Properties of Optoacoustic

Sources, Report Number AD-A133744 (Defense Technical Information Center, Alexandria, VA, issued September 1983).

D. Ph.D. dissertations supported by this contract.

1. D. S. Langley, "Light Scattering from Bubbles in Liquids" (Physics Department, Washington State University, July 1984).

E. Masters-Degree Project papers (Note: Washington State University allows for MS degree programs in physics and electrical engineering which have no requirement of a formal thesis. The students in these programs are required to submit a Project Paper which is reviewed by faculty members. Normally these papers are not distributed externally; however, they sometimes are the preliminary description of work which is eventually published.)

1. B. L. Brim, "Theoretical investigation of Brewster angle phenomena for curved surfaces" (Dept. of Electrical Engineering, Washington State University, August 1983).

II. Preface and Explanation of System of References

This report summarizes progress in research supported by the contract titled: "Propagation and Effects of Acoustical and Optical Waves." The emphasis of this report is on progress subsequent to that described in the report by P. L. Marston titled:

Technical Report No. 3. Focused Acoustical and Optical Backscattering from Spheres and Properties of Optoacoustic Sources (DTIC No. AD-A133744, issued September, 1983).

However, for continuity, certain research discussed in that report will be mentioned.

The following reference system is used in this report. References to recent external communications supported by this contract will be made by giving the section letter and number of the list given in Sec. I of the present report. For example, the first item listed in Sec. I is referenced as A1. Reference to other literature, including earlier work supported by this contract, are listed in Sec. VII. The first item in that list is referenced as [1].

Graduate students contributing to the work discussed in this report include Dean S. Langley, Bruce T. Unger, and Kevin L. Williams. The research of former graduate students including: Bradley L. Brim, Timothy J. B. Hanson, and Jeffrey L. Johnson, was either directly used and/or will merit brief description in this report. Colleagues at institutions other than Washington State University who have contributed to aspects of this research (without cost to the contract) include: James H. Crichton (Professor of Physics, Seattle Pacific University, Seattle, WA) and Eugene H. Trinh (Staff Scientist, Jet Propulsion Laboratory, Pasadena, CA).

III. Acoustical Scattering Theory and Experiments

A. Motivation for this Research

The motivations for this study of the scattering from elastic objects in water are as follows: (i) It is an example of the development and testing of new models for the scattering from elastic objects for cases in which diffraction provides essential corrections to elementary ray acoustics. Such diffractive corrections occur both with spherical and nonspherical objects where the scattering is strongest and in the reflections from extended curved surfaces. (ii) Our models consider focused backscattering from special spheres which should have giant backscattering cross sections.[1] Such spheres should be useful as calibration targets[2] or as passive navigational beacons.

(iii) Our models consider focused Rayleigh wave contributions to the scattering of elastic objects. Such contributions are particularly indicative of the size and/or composition of the scatterer. (iv) We are combining our modeling techniques (which use geometrical acoustics and diffraction theory) with other developments in scattering theory including "Resonance Scattering Theory."

One salient aspect of this research is our ability to model and measure scattering amplitudes not just in backward directions but also in near backward directions. It is shown that the diffraction lobes in near-backward directions are indicative of the target's size.

B. Focused backscattering from large elastic spheres:

Transmitted wave acoustical glories

In earlier work, we have shown that elementary geometrical acoustics predicts an infinite backscattered amplitude due to certain waves transmitted through a sphere but that diffraction theory may be used to remove this unphysical infinity.[1] The correctness of our model for certain classes of glory waves was experimentally confirmed using the apparatus diagrammed in Fig. 1. The first confirmation came from experiments[A1] which measured the backscattering due to unmixed-chord glory rays such as those diagrammed in Fig. 2 for a sphere of fused silica in water. Figure 3 is a representative comparison between measurements and theoretical predictions when $ka \simeq 457$ where a is the sphere's radius, $k = 2\pi/\lambda$, and λ is the acoustic wavelength in water. The spacing of the diffraction maxima and minima in near backward directions are indicative of the size and composition of the scatterer.

We have recently extended both the model and the experiments to the much more difficult problem of the "mixed-mode" or "mixed-chord" acoustical glory from an elastic sphere in water.[A8] Our previous model[A1] was complete

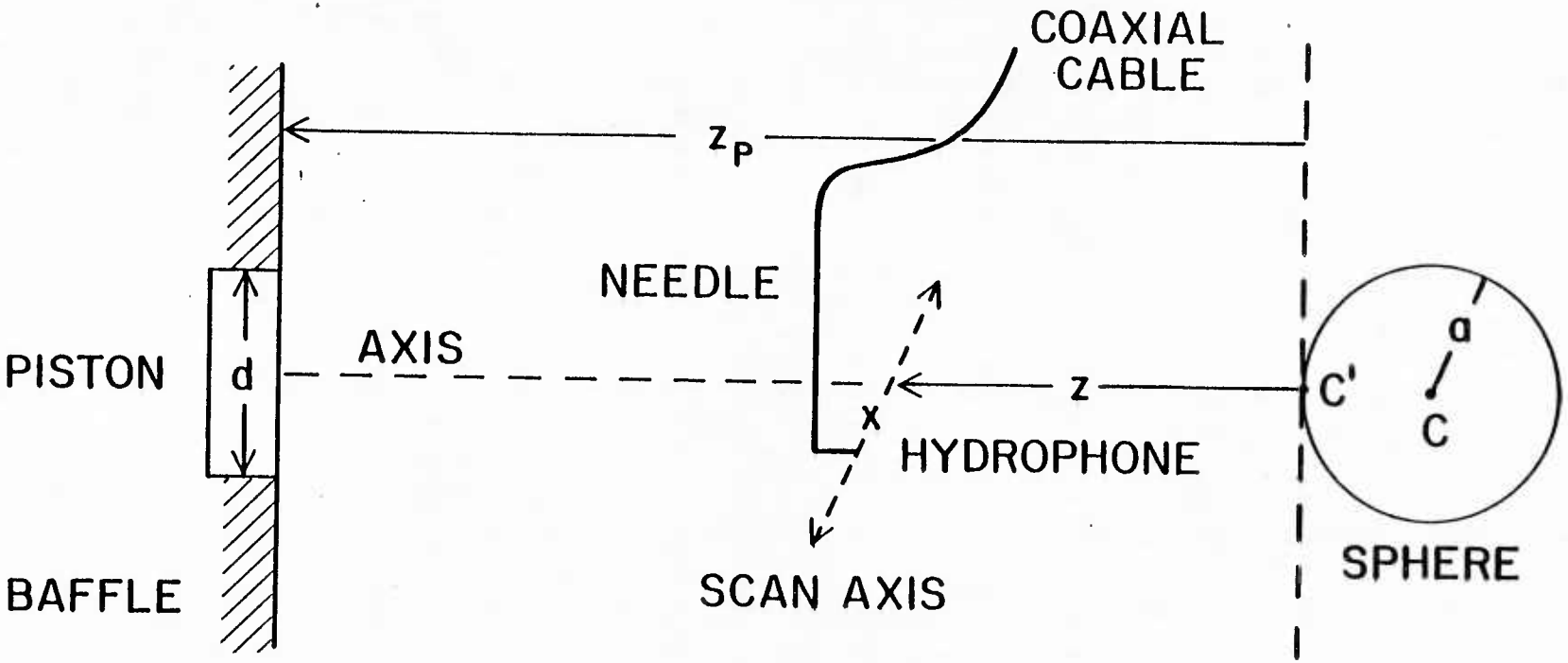

Fig. 1. Simplified diagram of the scattering experiments. The hydrophone may be scanned along a line transverse to the symmetry axis defined by the source and the sphere. The diagram is not drawn to scale.

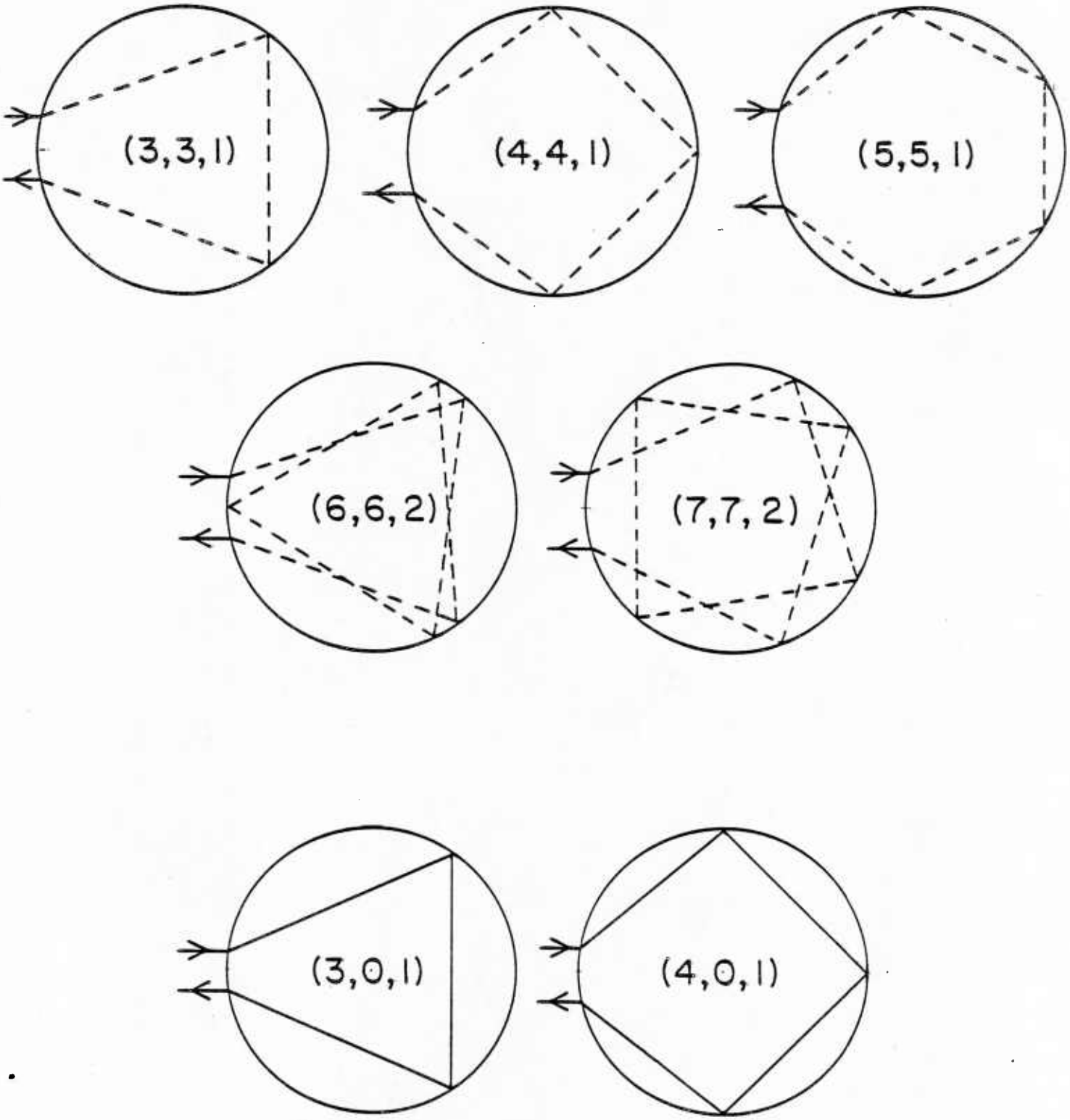

Fig. 2. Representative unmixed-chord glory rays for a fused-silica sphere in water. Dashed and solid rays represent shear and longitudinal waves, respectively.

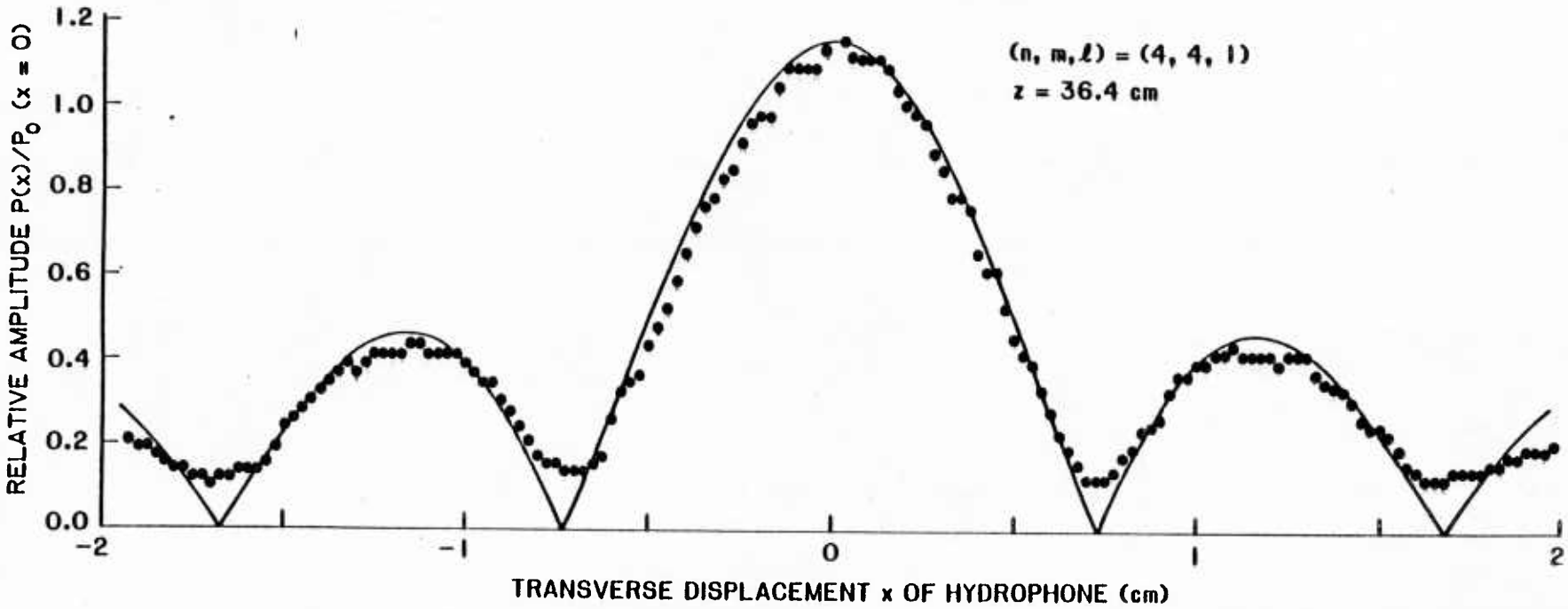

Fig. 3. The peak-to-peak voltage for the (4,4,1) echo plotted as a function of x. The voltages are ratioed with the on-axis value of the first axial echo. Measurements were obtained when the water temperature was 24.9° C. The solid curve is the modeled dependence on x = 0. The peak at x = 0 and the side lobes are direct evidence of axial focusing.

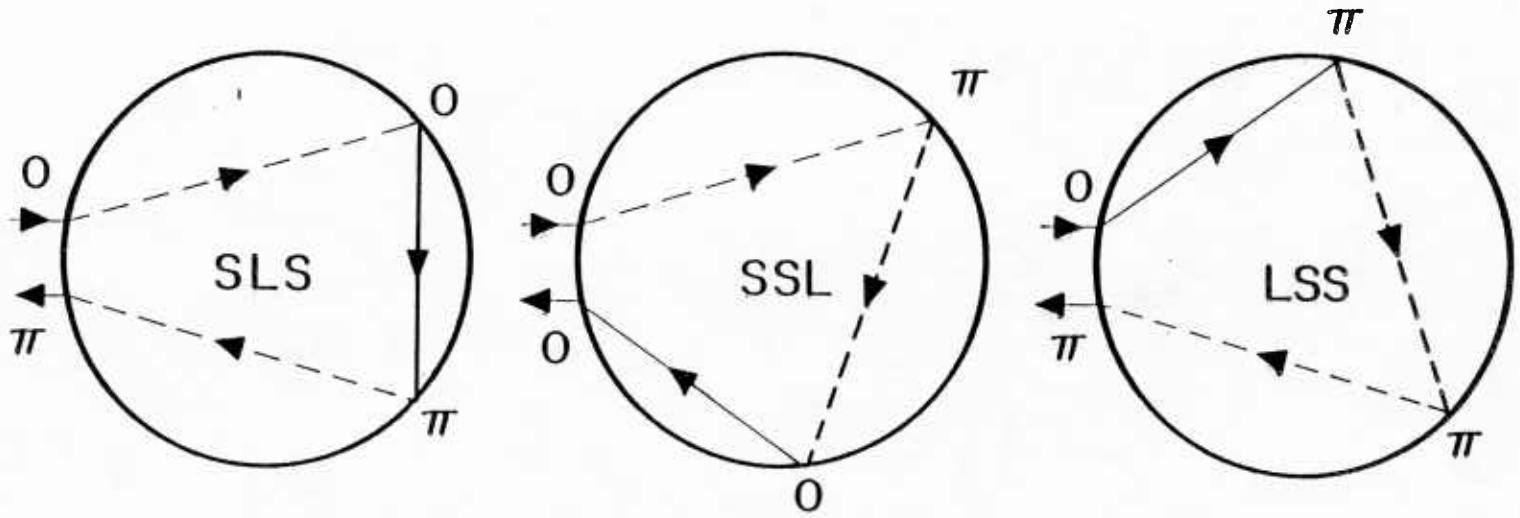

Fig. 4. The three chord sequences associated with the (3,2,1) mode of a silica sphere in water. The arrows indicate directions of propagation. The quantities (0 or π) at each vertex are the phase shift ψ_k due to transmission and reflection.

Table I. Predicted and Measured On-Axis Pressure Ratios for the (3,1,1) and (3,2,1) Echoes at Two Different Receiver-Sphere Distances. Also shown is B_σ and Ψ_σ for each chord sequence at both echoes. The water temperature was 20°C.

	Chord Sequence	B_σ	Ψ_σ	z = 34.8 cm $\mathcal{R}_E$	$\mathcal{R}_T$	$\mathcal{R}_E/\mathcal{R}_T$	z = 113.6 cm $\mathcal{R}_E$	$\mathcal{R}_T$	$\mathcal{R}_E/\mathcal{R}_T$
(3,1,1)	LSL	0.1781	π	0.841±0.008	0.865	0.972±0.009	0.907±0.033	0.908	0.999±0.037
	LLS	0.0207	3π						
	SLL	0.0207	π						
(3,2,1)	SLS	0.1496	2π	0.502±0.004	0.525	0.956±0.008	0.552±0.021	0.551	1.002±0.037
	SSL	0.0213	π						
	LSS	0.0213	3π						

only for transmitted waves within the sphere which were either all longitudinal (L) or all shear (S). In this new research we completed the theory for the case of mixed-mode echoes in which there is at least one L-to-S or S-to-L mode conversion due to internal reflection. The chord sequence of one of the mixed modes studied is shown in Fig. 4. A novel calculation shows that the focal parameters are independent of permutations of the mode sequence; however, the contributions to the scattering depend on sequence. That a phase factor Ψ_σ and an amplitude factor B_σ depend on the sequence is shown by the theoretical values tabulated in Table I. The full expressions for the amplitude and phase are given in Ref. A8. For the purposes of the present discussion it is important to note that a correct prediction for the mixed-mode amplitude is only possible if the interference between the different sequences contributing to that mode are properly modeled.

Data which confirms our model of the mixed-mode backscattering is displayed in Table I. $\mathcal{R}_E$ and $\mathcal{R}_T$ are experimental and theoretical amplitudes, respectively, which are normalized to the amplitude of the first specular reflection from the sphere. In some cases the agreement between experiment and theory is seen to be better than 1%. Data acquisition and analysis was made possible by using a digital signal averager and a digital tone burst generator both purchased with contract funds.

C. Axially-focused (glory) backscattering due to Rayleigh waves generated on elastic spheres.

For most sonar systems and targets, the ka is significantly smaller than the ka of the aforementioned experiments on transmitted-wave glories. It may be argued that when ka < 100 certain radiation damped "surface" waves will significantly contribute to the backscattering from elastic spheres or spherical shells. Which type of surface wave, and their relative strengths,

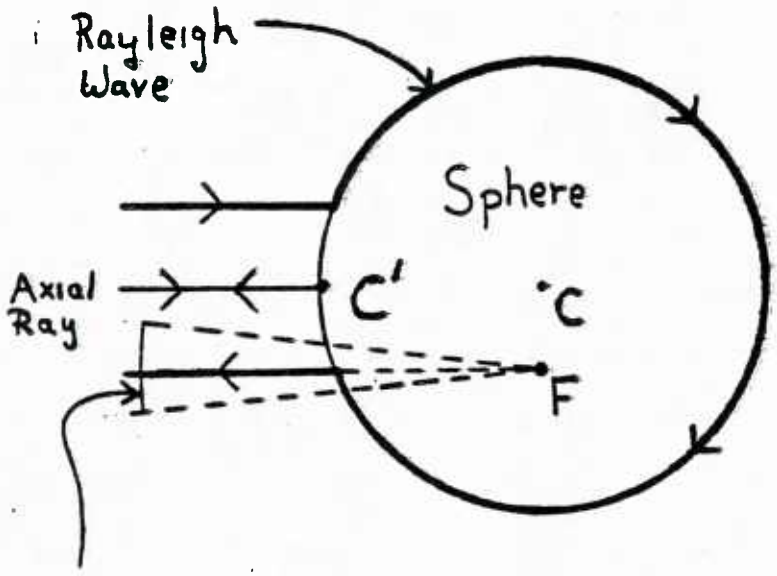

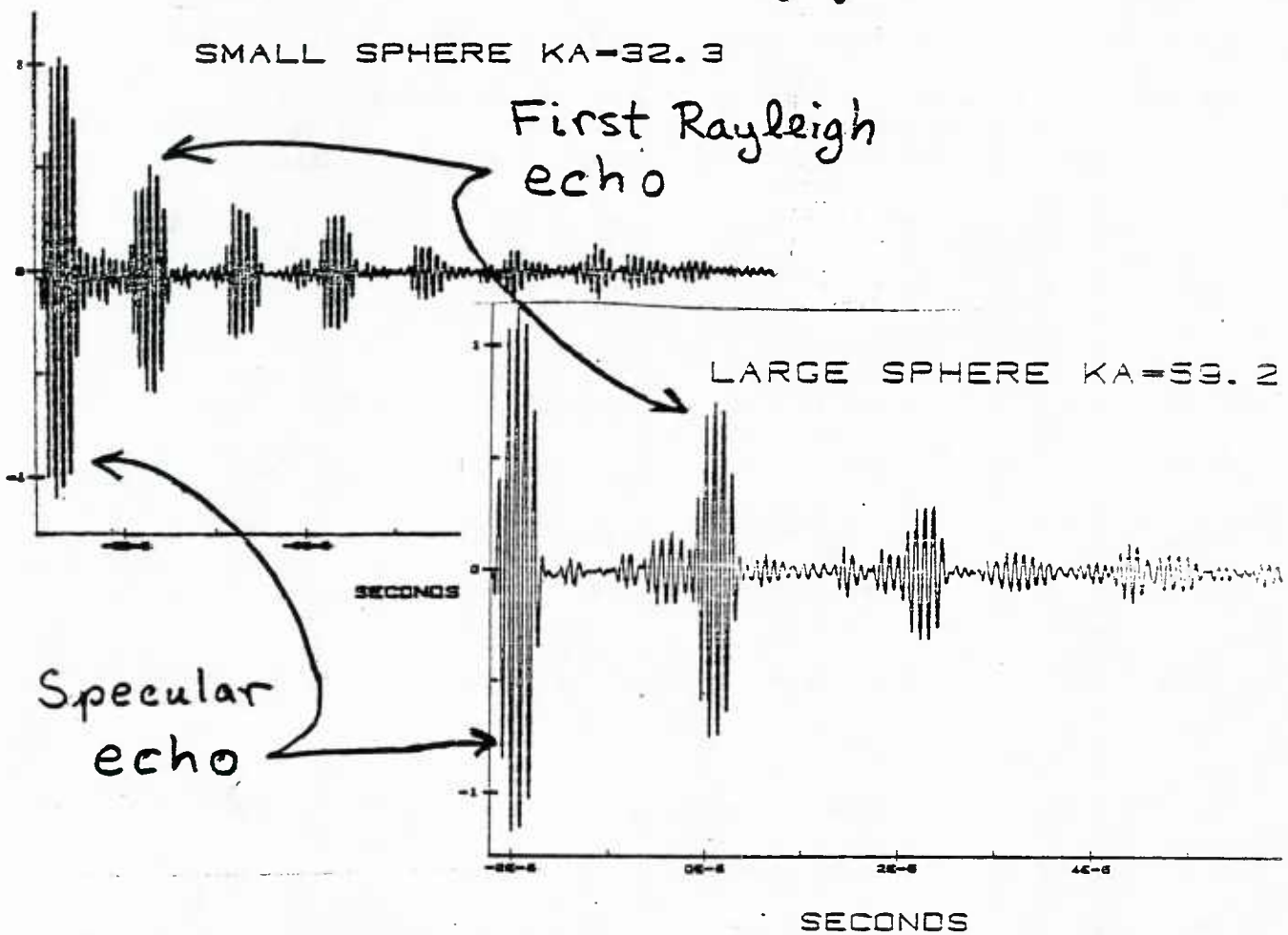

Fig. 5. The upper figure shows the ray path which results in a Rayleigh wave on the sphere and a backscattered toroidal wave. The point F is on the focal circle associated with the toroidal wave. The (unfocused) axial ray is also shown. The lower curves show the received pulse trains (when the hydrophone is placed at x = 0 in Fig. 1) for a tungsten-carbide sphere (in water) in response to incident tone bursts of the indicated ka.

will depend on the physical nature of the scatterer. It is of general interest both to demonstrate (and to model) the axial-focusing of backscattering due to surface waves. We have measured and modeled the particular case of scattering from tungsten carbide spheres in water in the range: $30 \leq ka \leq 100$. The dominant surface wave in this range is the Rayleigh-like wave. The angular dependence of its contribution to the scattering was modeled and the model was confirmed with measurements.[B7] The angular dependence is indicative of the sphere's size.

The experiments were carried out with the measurement configuration diagrammed in Fig. 1. The apparatus was changed (from that used in our previous work[1,A8]) to extend its bandwidth and reduce its operating frequency by changing the transducers and the preamplifier. The tungsten carbide spheres had diameters of 1 inch and 0.5 inches. When a short tone burst is incident on a tungsten carbide sphere, the backscattering response shows a decaying pulse train which can be attributed to a specular reflection and the repeated circumnavigations of waves. Representative cases, measured with our apparatus, are shown in Fig. 5. The specular and first-Rayleigh-wave contributions to the backscattering are identified. The general appearance of these curves are similar to a measurement of the transient backscattering published by the group at the Naval Research Laboratory.[3] In the NRL measurement, however, the incident sound was not a well defined burst of sine waves (as in Fig. 5) and the angular dependence of the scattering (discussed below) was not described.

If the receiver is moved away from the backscattering axis, the amplitude of the Rayleigh wave contribution at first decreases, and then undergoes an oscillatory dependence on the transducer displacement x. We have developed a theory for the angular dependence which predicts the Rayleigh wave

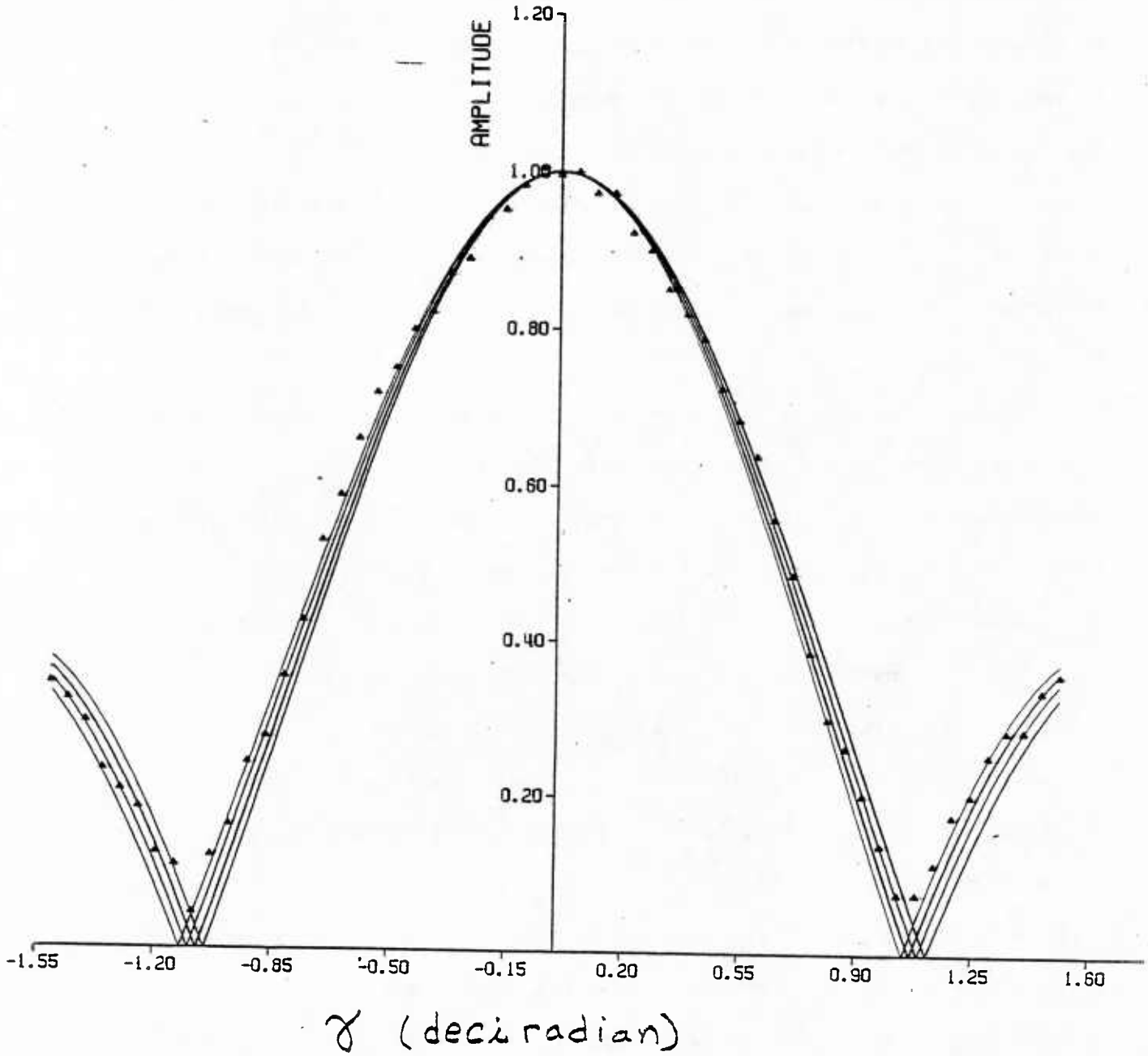

Fig. 6. Measured scattering amplitude (due to the first Rayleigh wave) normalized to the value at $\gamma = 0$ and plotted as a function of the backscattering angle γ. The data points are for ka = 59.2. The curves are the form predicted for an axially-focused wave (Eq. (1)) for several different values of the focal parameter β.

contribution to the scattered sound has a pressure amplitude which satisfies the following proportionality:

$$p_{Rayleigh}(ka,\gamma) = p_{Rayleigh}(ka,\gamma=0)J_0(\beta\gamma), \quad (1)$$

where $\gamma = \tan^{-1}(x/(z+a))$ is the angle relative to the backscattering axis, $<< 1$ radian, and J_0 is a Bessel function. The constant β is predicted to depend on the frequency of the sinusoidal tone burst used (or equivalently the ka of the sphere). The general reasoning leading to Eq. (1) is similar to that which we give in References 1, A1, and A5 for other cases of axially-focused scattering: the scattered pressure wave in the water appears to emanate from a virtual ring-like source which we call the focal circle. We first tested the proportionality on $J_0(\beta\gamma)$ by measuring the dependence of Rayleigh amplitude and plotting the ratio

$$\mathcal{R} = \frac{|p_{Rayleigh}(ka,\gamma)|}{|p_{Rayleigh}(ka,\gamma=0)|} . \quad (2)$$

Representative data points for the case ka = 59.2 are shown in Fig. 6. An empirical value for β, call it β_E, was determined by adjusting $J_0(\beta_E \gamma)$ to best fit these data. This procedure is also illustrated in Fig. 6 which shows that these data are of the expected form. Using this empirical β_E, Eq. (1) predicts the first null (where $p_{Rayleigh}(ka,\gamma_1) = 0$) to be at:

$$\gamma_1 \simeq \frac{2.4048}{\beta_E} \text{ radians} . \quad (3)$$

We have also developed a theory for β which is based on finding the focal-circle radius from a phase matching condition. The result is

$$\beta = ka\, c/c_p , \quad (4)$$

where c is the velocity of sound in water and c_p is the phase velocity of the Rayleigh wave on a tungsten-carbide sphere in water determined at the ka of the incident tone burst. The procedure for calculating c/c_p is complicated and will only be briefly summarized. An extension of the theory of resonance scattering (Ref. 4, Eq. 46c) gives c/c_p as

$$\frac{c_p}{c} = \frac{\mathrm{Re}(X_{n,1})}{n + (1/2)} , \tag{5}$$

at discrete values $ka = \mathrm{Re}(X_{n,1})$. Here $X_{n,1}$ is the Rayleigh complex root of the following equation

$$D_n(X_{n,1}) = 0 , \tag{6}$$

in which D_n is the following determinant

$$D_n(X) = \begin{vmatrix} d_{11} & d_{12} & d_{13} \\ d_{21} & d_{22} & d_{23} \\ 0 & d_{32} & d_{33} \end{vmatrix} , \tag{7}$$

and the $d_{ij}(X)$ in this determinant are the complex functions listed in the Appendix of Ref. 5. The d_{ij} are functions of X involving spherical Bessel and Hankel functions, j_n and h_n, their derivatives, and the elastic parameters of the sphere and of the surroundings (water). Equation (6) was solved numerically for the roots $X_{n,1}$ for the partial-wave index n having integer values from 4 to 30. This procedure (carried out by Kevin Williams) was facilitated by adapting computer programs previously implemented by B. L. Brim during previous contract related research.[E1] The values of $X_{n,1}$ agreed with those given in Table IV of Ref. 5 for the specific cases $n = 4$ to 7. The c_p/c values thus obtained from Eq. (5) for discrete $ka < 85$ were fitted

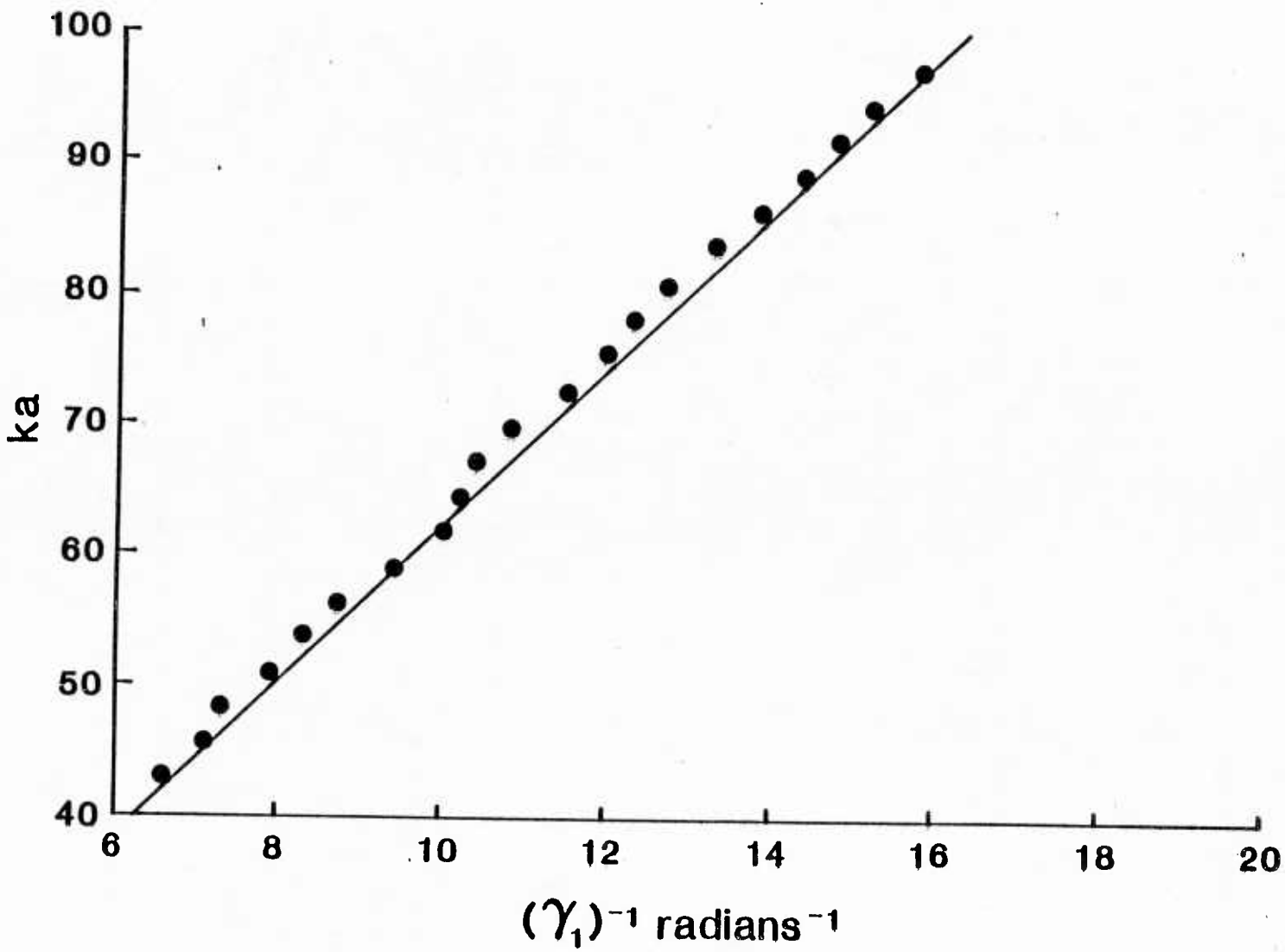

Fig. 7. The horizontal axis is the reciprocal of the first null angle γ_1 for the value of ka shown on the vertical axis. The theory (solid line) and measurements (circles) are for the first Rayleigh echo from a tungsten-carbide sphere in water.

with a polynomial to give c_p/c as a continuous function of ka over the ka-range of interest.

The aforementioned procedure, together with Eqs. (1) and (4), gives the following theoretical value for the null angle

$$\gamma_1 = \frac{2.4048}{ka} \left(\frac{c_p}{c}\right) \text{ radians} . \tag{8}$$

Figure 7 compares the theoretical $(\gamma_1)^{-1}$ (solid line) with the experimental values (circles) from Eq. (3). The ordinate is the ka value for the incident burst. The agreement between theory and experiment is sufficient to confirm the principal features of our model of the angular width of the focused backscattering.

There may be a small systematic source of error in the theoretical calculation displayed in Fig. 7 because the elastic properties of the specific tungsten carbide samples used in this experiment were not precisely known. Calculations of c_p/c based only on tabulated elastic properties were adjusted to according to the measured group velocity c_g for these spheres according to a relation between c_g and c_p derived by Williams for the ka region of interest. The resulting theory line is the one shown in Fig. 7. If only previously tabulated elastic properties are used, the revised theory line has a slightly larger slope. The theory lines computed with and without the aforemention correction bracket the data.

Though the experiments we described here, and in Sec. IIIC, use incident tone bursts of only a few cycles in length, the concept of axial focusing is also applicable to spheres or spherical shells insonified by long incident tone bursts. For example, certain large resonance features in the scattering from spherical shells[6] may be attributed to a particular partial

wave, say the nth partial wave. The angular dependence of the amplitude for the nth partial wave may be expanded using Szego's asymptotic expansion of the Legendre polynominal[A1]

$$P_n(\cos\gamma) \simeq J_0[(n + \tfrac{1}{2})\gamma] \ , \tag{9}$$

when $n \gg 1$ and $\gamma \ll 1$ radian. This is of the same form we have demonstrated here in Fig. 3 and 6 for selected responses to short tone bursts.

D. Nearfield effects in acoustic scattering

We have investigated aspects of the nearfield-to-farfield transition for the backscattering from an elastic sphere. The motivation for this research is as follows: (i) Following a presentation (at the Acoustical Society of America Meeting, Orlando, FL, Nov. 1982) of our research,[7,A1] questions were raised by a member of the audience concerning the theoretical form (Eq. 10, below) used to model the specular (i.e., first axial) contribution to the scattering. A detailed derivation of this result was subsequently published as an insignificant part of Ref. A1. However, it is not too surprising that our model of the specular reflection is not well known since it differs in detail with that used in the NRL study of calibration spheres.[3] (ii) There has been recent interest[7] in the criterion for establishing the farfield in scale model scattering experiments.

With reference to Fig. 1, our model for the amplitude of the first axial (or specular) reflection for a tone burst having $ka \gg 1$ is[A1]

$$|p_0| = |p_{inc}| \frac{a}{2(z + \frac{1}{2}a)} R_{WW} e^{-\alpha z} \ , \tag{10}$$

where: a is the sphere's radius; $|p_{inc}|$ is the pressure magnitude of the

incident tone burst measured at point C' in Fig. 1; α is the attenuation coefficient of sound in water for the central frequency of the tone burst; and $R_{WW} = (\rho_i c_L - \rho_o c_W)/(\rho_i c_L + \rho_o c_W)$. Here ρ_i and ρ_o (and c_L and c_W) are respectively the densities (and longitudinal sound speeds) of the elastic sphere and of water. The feature at question here are the $(z + \frac{1}{2} a)^{-1}$ divergence factor which shows the reflection appears to emanate from a point-like source located half-way between C' and C in Fig. 1. Also important is our assertion that R_{WW} is less than unity in Eq. (10). Our derivation of Eq. (10) assumes not only that $ka \gg 1$ but also that the source distance $z_p \gg a$ and that the (small) receiver hydrophone is located on the backward axis at $x = 0$ in Fig. 1.

To test the correctness of Eq. (10), measurements were made of the specular amplitude $|p_0|$ at several distances z from a fused silica sphere having $a = 51.6$ mm. The z ranged from 6 cm to $\sim$95 cm. The frequency of the incident tone burst was 2 MHz. Comparison of the measured $|p_0|/|p_{inc}|$ with the predictions of Eq. (10) clearly demonstrate that $(z + \frac{1}{2} a)^{-1}$ is the correct divergence factor in Eq. (10). Indeed, if $(z + \frac{1}{2}a)^{-1}$ is replaced by $(z + a)^{-1}$ (which is the form often assumed in farfield models of the scattering), the modified theory quite clearly disagrees with the data, especially for $z < 50$ cm. Note that $(z + a)$ is the distance of the hydrophone from the sphere's center.

In related developments, we have previously noted[1,9a] that a general farfield condition of

$$z \gg ka^2 \tag{11}$$

follows from the requirement that the farfield is the region where

Fraunhofer's approximation to diffraction integrals is applicable. We have also shown Eq. (11) by answering the question: "When are farfield approximations applicable in exact partial-wave theories for the scattered field?" Surprisingly the condition (11) does not appear to be well known since the principal investigator (P. L. Marston) recently refereed a manuscript concerned with nearfield scattering in which (11) was evidently not known to the author even though his calculations supported this result! At Marston's suggestion, a discussion of Eq. (11) included and the manuscript was published as Ref. 9b. The condition Eq. (11) should be a sufficient condition in acoustic scattering from bounded nonspherical objects provided a is taken to be half the largest width of the object.

E. Backscattering from a large torus: a simple example of axial focusing

The scattering from a large torus was modeled for the case of an incident plane wave which propagates parallel to the symmetry axis of the torus.[A5] The configuration modeled is shown in Fig. 8. In this case the specularly reflected wave is axially focused; it appears to emanate from a focal circle (at F_0 in Fig. 8). For a large rigid torus the pressure of the reflected wave is predicted to be[A5]

$$p_o = \left(\frac{p_{inc}\, b}{r}\right) (\pi ka)^{1/2} J_0(u_0)\, e^{i\left(kr + \varphi - \frac{\pi}{4} - \omega t\right)}, \qquad (12)$$

where: $u_0 = kb\sin\gamma$; a and b are as shown in Fig. 8; the polar coordinates (relative to C') of the observation point are r and γ; $\varphi = -ka(1 - \cos\gamma)/2$; and p_{inc} is the amplitude at C' of the incident plane wave.

This model was developed so as to identify an example of focused backscattering which would be free of some of the intricacies of the modeled scattering from spheres.[1,A1] Observations of scattering from a torus would be

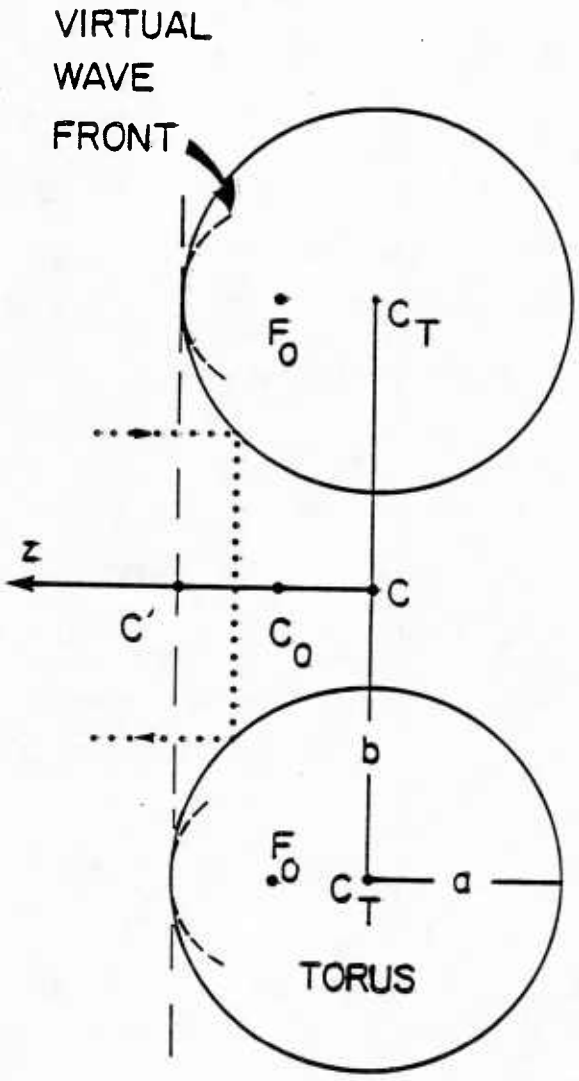

Fig. 8. Cross-sectional view of the rigid torus for which the backscattering was modeled. The figure may be rotated about the CC' axis. The reflected wave is axially focused along the left extension of the CC' axis when the incident wave propagates in the -z direction. Scattering due to the dotted ray is omitted.

particularly useful in testing a model[A5] of pulse distortion which results from focusing. There are, however, other potential applications which include: (i) the use of a torus as either a calibration target or as a navigational target because of the simple form manifest in Eq. (12); (ii) the use of a torus as a special case in which to test computational algorithms for the scattering from objects having large aspect ratios. (There have been recent advances[10] in the development of algorithms applicable to prolate scatters having large aspect ratios and similar advancements for the case of oblate scatters are to be anticipated.) Unless the conditions ka >> 1, kb >> 1, and b >> a are all met, however, in addition to (12) there will be other significant contributions to the backscattering including those due to the dotted ray in Fig. 8 and to surface waves which loop around either side of the torus.

F. Theory of pulse distortion in focused scattering: half-order derivative of a sine-wave burst

An important property of focused scattering, such as that discussed in Sec. IIIB and IIIE of this report, is its large magnitude. Then it is reasonable to inquire whether certain features of a scattered transient are indicative of focused scattering If such features were unmistakable, it would be possible to discriminate between sonar targets which were large in size (and having no focused backscattering) and targets which were small (whose signals were large because of focusing of the backscattering). Our calculation of the half-order derivative of a sine-wave burst[A5] is a step toward the resolution of questions of this type. In our model of focused high-frequency scattering from spheres,[A1] it was found that certain of the axially focused waves had pressures proportional to

$$\left(\frac{d}{dt}\right)^{1/2} s(t) = \int_{-\infty}^{t} \dot{s}(\tau)[(t-\tau)\pi]^{-1/2} d\tau , \qquad (13a)$$

where $\dot{s}(\tau) = ds/dt$ at $t = \tau$ and $s(t)$ is proportional to the pressure of the incident wave p_{inc}. In the present calculation the incident wave was modeled as a burst of sine waves N cycles in length so that $s(t)$ could be written as the product

$$s_N(t) = H(\omega t)H(2\pi N - \omega t)\sin\omega t , \qquad (13b)$$

where the Heaviside unit-step function

$$H(y < 0) = 0, \; H(y > 0) = 1, \text{ and } H(y = 0) = 1/2.$$

It was found by direct evaluation of Eq. (13) that $(d/dt)^{1/2} s_N$ may be expressed using a combination of phase advanced sine waves and the auxiliary Fresnel-integral function.[A5] The leading edge of a focused burst is steepened and the peak amplitude of the first half-cycle is suppressed. The trailing edge of the focused burst is predicted to manifest a tail. Before recent improvements in our experimental apparatus, Fig. 1, the bandwidth of our system was judged to be insufficient to experimentally test these predictions in detail. Results of this calculation for the central peak-to-peak amplitude of a focused burst having $N \geq 4$ justify the experimental procedures used in the confirmation of theory in Refs. A1 and A8.

In addition to aforementioned motivations for the evaluation of Eq. (13), the following should be noted. It would be possible to compare these results with those of an "exact" calculation of the scattering of a burst based on the evaluation of the partial-wave series at many discrete frequencies and the use of a fast-Fourier-transform algorithm. Such an exact

computation is sufficiently intricate that the comparison of results with simple models (for special cases) is justified.

IV. Scattering of Light from Bubbles in Liquids and Other Problems in Electromagnetic Scattering of Value to Acoustics and Naval Technology

A. Motivations and Overview

The majority of the contract research into electromagnetic scattering is concerned with the optical properties of bubbles in liquids. In this section some motivations for understanding the scattering properties of bubbles will be noted.

Gas bubbles of natural origin inhabit the upper layers of the ocean;[11] however, the causes, lifetimes, and size spectra of these natural bubbles are not well understood.[12] Medwin's acoustic measurements suggest that the bubbles may be present in large numbers even at depths of 36 meters where he estimated (Fig. 6 of Ref. 11) there to be, for example, ~ 8000 bubbles/m^3 in the radius interval 65 to 66 μm. Bubbles also affect the colors of the sea in regions of breaking waves,[13] and the optical properties of sea ice.[14]

Bubbles are important to various naval technologies. For example, natural bubbles may result in fluctuations of the acoustic properties of the near-surface ocean (Ref. 11 and papers cited therein). Man made bubbles may be injected in the ocean to regionally reduce the transmission of sound[15,16] (the "bubble screen" technique.) Microbubbles also govern the inception of acoustic and hydrodynamic[17] cavitation. Microbubbles alter the effective nonlinearity parameter (B/A) of a liquid and also the generation of acoustic 2nd harmonics and parametric signals (having the sum or difference frequency of the pump waves). Hydrodynamic flow drag may be reduced by the injection of microbubbles (through a porous section of the wall) into the liquid boundary layers.[17] Bubbles are also useful as tracers in hydrodynamics research.[18]

Bubbles may also be significant in optical communications and/or detection technologies involving submerged platforms.

In spite of the aforementioned significance of bubbles (and other applications noted below) no systematic research into the optical scattering properties of bubbles had been carried out prior to the present ONR Contract research which began in 1980. Critiques of the research prior to about 1980 are given in Ref. A4, A9, A10, 19, and 20 and we need only summarize them. The principal modeling approaches had been based on geometrical optics[21] and significant effects of interference and diffraction were not included. Such models might appear to be reasonable since bubbles are usually much larger than the wavelength of light λ_o in water; we find, however, that geometrical methods by themselves are deficient even for large spherical bubbles. Deficiencies are evident in the various transition regions of the scattered light, particularly in the near forward and backward directions[20,22] and in the critical-angle region[19,A4] where the transition from partial to total reflection at the bubble's surface occurs. In the light of our Mie calculations[19] (which are exact for spheres), physical-optics approximations,[23] and (now) data[A4,A10] the early (1972) Mie calculations of A. Keller[24] appear to be erroneous. (We mention this because Keller's research is still used to justify certain optical technologies for counting bubbles in cavitation research.[17])

In the present research we continue to model bubbles as spherical voids surrounded by a homogeneous dielectric media (usually water). Some recent data support this assumption for small bubbles in clean or moderately lean water. Even with the simplification of an assumed spherical shape, the backscattering properties of bubble-like objects were not considered by previous research into short-wavelength scattering (including, e.g. well known

previous research into short-wavelength scattering (including, e.g. well known papers by Rubinow,[25] Nussenzveig,[26] and Inada and Plonus[27]).

There is already evidence that the present line of research has affected existing or future technologies relating to the measurement of bubble size spectra in the ocean,[12,28] the measurement of bubble sizes in acoustics cavitation research,[29] and the modeling of bubbles in glass (as applied to high-power laser glass amplifiers[30]). It is likely to affect research on bubble nucleation in polymer liquids (as applied to plastics technology[31]).

The emphasis of this research has been on the understanding of fundamental scattering properties of bubbles as noted in Sec. IVB-IVD of this report. These properties are relevant to various bubble detection and sizing technologies. We also model a novel application in acoustics in Sec. IVE: the potential use of light scattering to directly measure the response of a bubble to an acoustic wave (or waves). The understanding of backscattering properties may be helpful in the evaluation of optical technologies to detect persistent bubbles in wakes which may be feasible in ocean regions (e.g. the Arctic) where background light scattering is less significant. (Bubbles in wakes have been asserted to have anomalously long lifetimes.) The understanding of glory-enhanced near-forward scattering is related to the degradation of the polarization of circularly polarized light incident on bubbly liquids.

The motivation for other optical scattering research is noted in Sec. IVF-H.

B. Critical angle scattering of light from bubbles

Our principal recent work on critical-angle scattering is the analysis and publication[A4,A10] of irradiance measurements for the angular region 68 to 85 degrees and bubbles ranging in radius from 26 to 986 μm. This angular

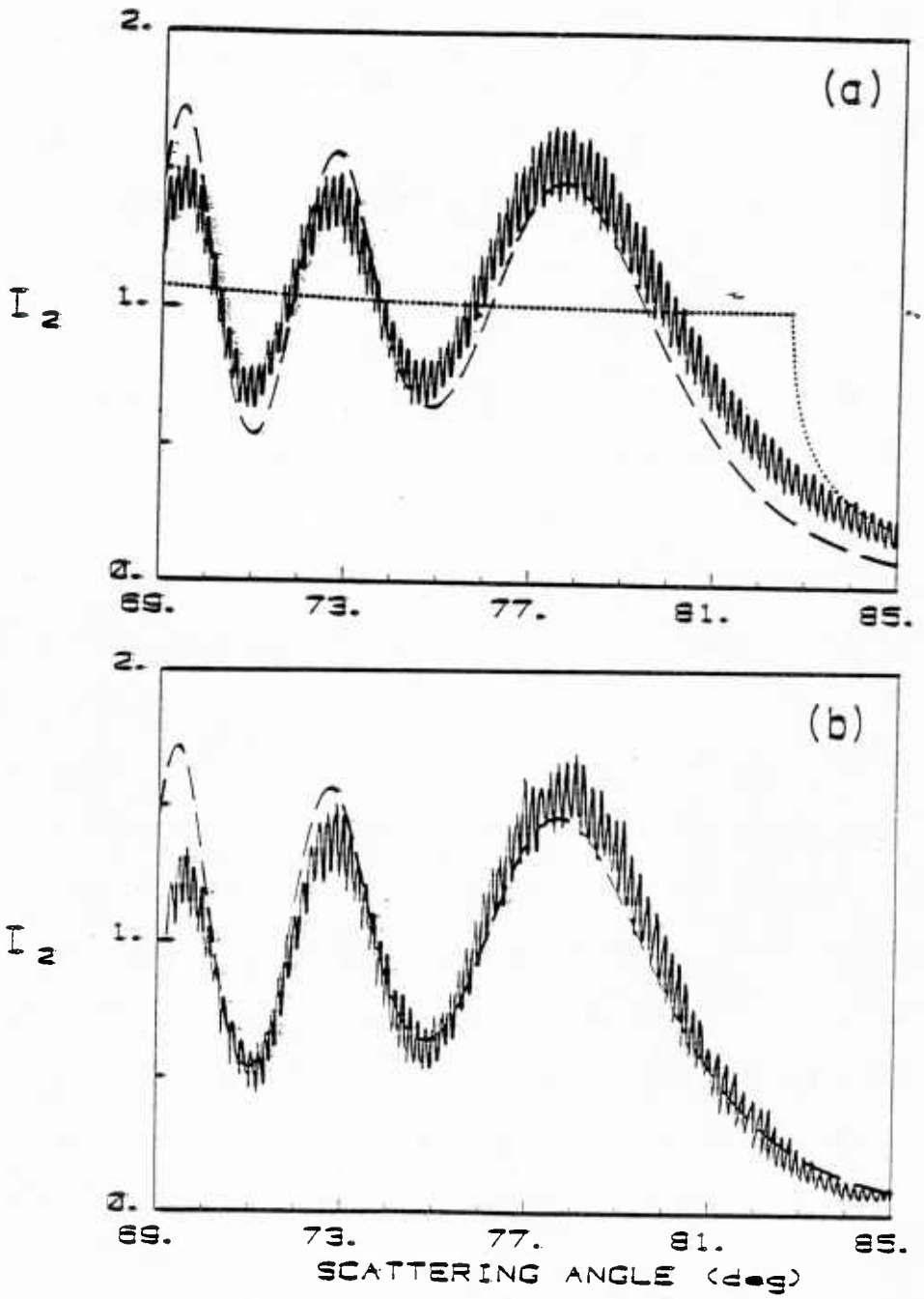

Fig. 9. Normalized scattered intensity from a bubble with ka = 1633 and the electric field parallel to the scattering plane. (a) Three models: the solid curve is the Mie theory, the dashed curve is a physical-optics approximation, and the dotted curve is from simple geometric optics. (b) The solid curve is experimental data and the dashed curve is the physical-optics model.

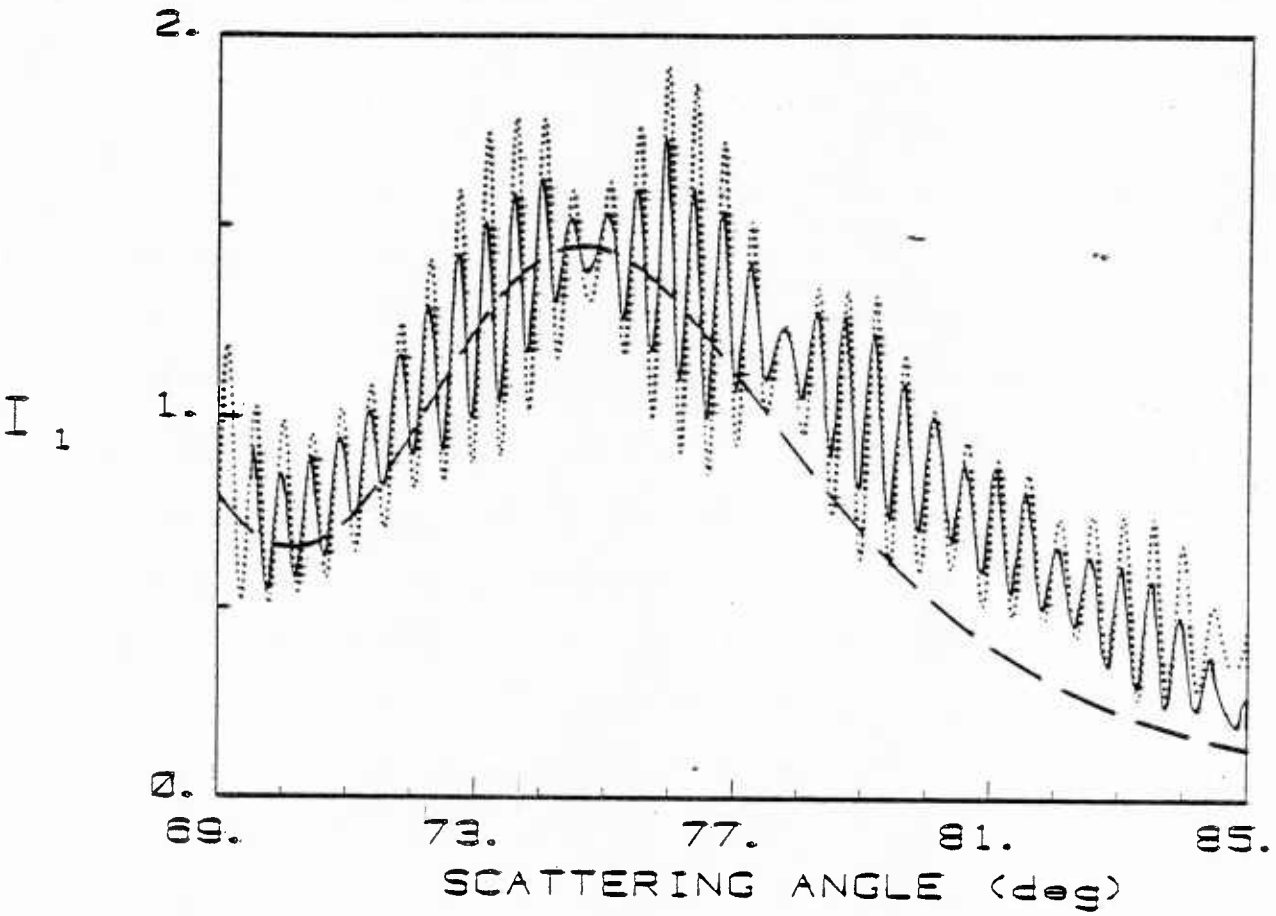

Fig. 10. The scattered intensity for ka = 612 when the electric field is perpendicular to the scattering plane. The solid curve is data, the dotted curve is the Mie result, and the dashed curve is the physical-optics model. The data indicate the bubble radius was 0.0461 $\pm$ 0.0001 mm.

region includes the transition to near-total reflection from the bubble's surface as well as the coarse oscillations of the intensity which result from interference and diffraction.[23] The incident light was a linearly polarized expanded beam of a He-Ne laser. Figure 9(a) compares various theories for the scattering in this region for a bubble having a radius a = 0.1235 mm such that $ka = 2\pi a/\lambda_o = 1633$. The dashed curve is the Marston-Kingsbury approximation.[23] The dotted curve, which is based on geometrical optics,[21] has an unphysically-divergent derivative at the critical scattering angle of 82.7 deg. Figure 9(b) compares our measurements for a bubble having a = 0.12 mm with the results of the Marston-Kingsbury approximation. The agreement is representative of measurement versus model comparisons for six bubbles in the size range 0.046 mm to 0.733 mm published in Ref. A4. It is also representative of comparisons based on measurements for 12 other bubbles which are displayed in Langley's Ph.D. dissertation.[D1] These comparisons, while confirming the basic features of the Marston-Kingsbury model, also reveal its nonuniform nature[A4] for scattering angles > 82 deg.

For the bubble having a = 0.046 mm measurements were compared with the detailed results of Mie theory. This comparison, Figure 10, shows that Mie theory correctly predicts the locations of both the fine structure and the contrast modulations of the fine structure. The success of Mie theory to predict these details of the measurements is evidence of the sphericity of the freely rising bubble. The comparison also suggests that the bubble's radius a was known to within $\pm$ 0.1 μm. See the Applied Optics publication.[A4]

One of the difficult aspects of Langley's experiment was the development of a precise angle calibration procedure. Figure 11 shows the apparatus during the angle calibration phase. Another important technique used was the trapping and direct radius measurement of single bubbles after

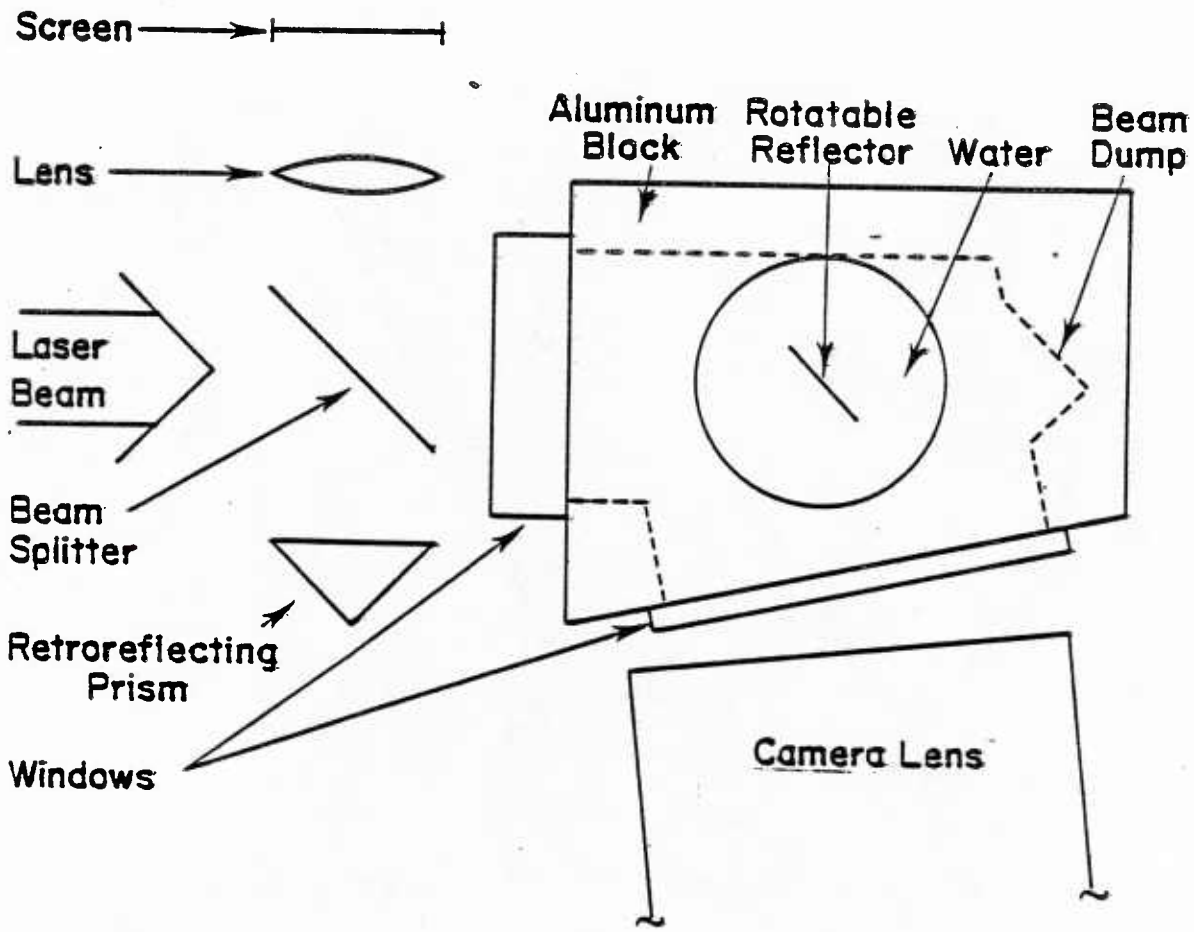

Fig. 11(a). Top-view diagram of apparatus set up for angle calibration. To observe bubble scattering the rotatable reflector was removed and bubbles were injected by a needle entering the bottom of the aluminum block. A microscope above the top opening was used to measure bubbles. The screen (used during angle calibration of the rotatable reflector) is at the optical-transform plane of the lens. The systematic uncertainty in the angle calibration was $< 0.02^{\circ}$.

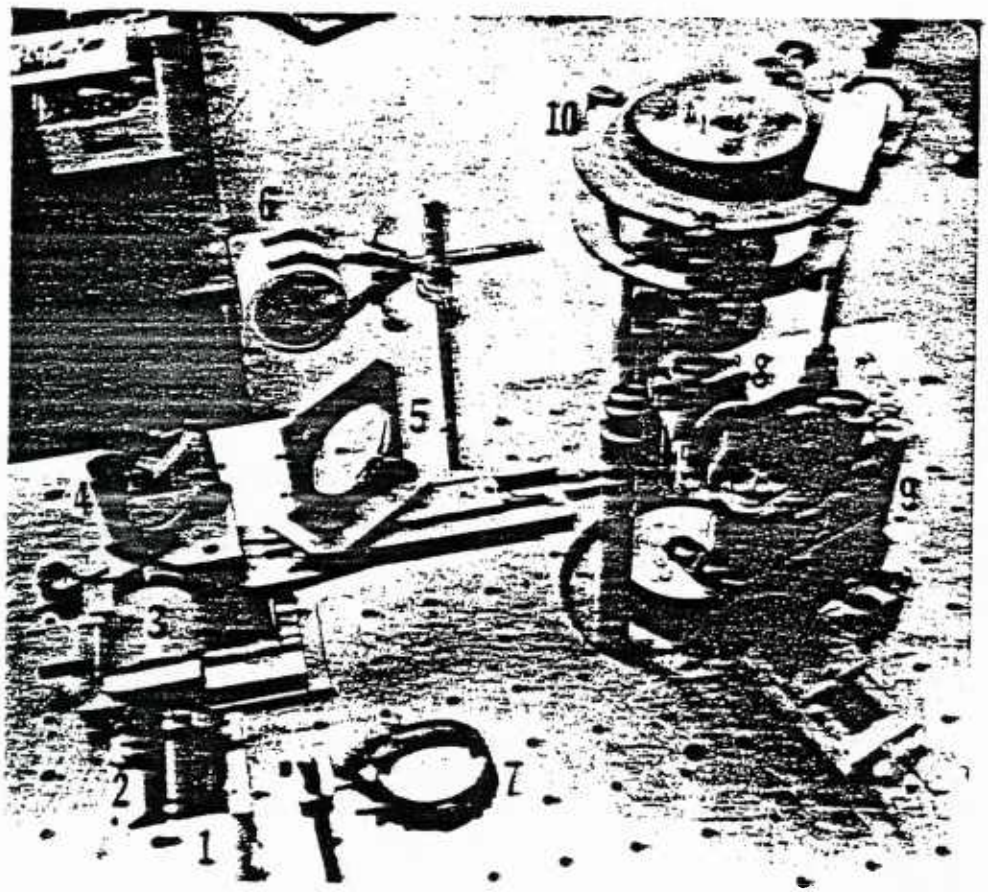

Fig. 11(b). Photograph of the experimental apparatus. The numbered devices are: (1) front end of laser, (2) beam expander, (3) polarization rotator, (4) mirror, (5) beam splitter, (6) retroreflecting prism, (7) lens, (8) scattering chamber, (9) camera, (10) mechanism of angle-calibration goniometer and rotatable reflector.

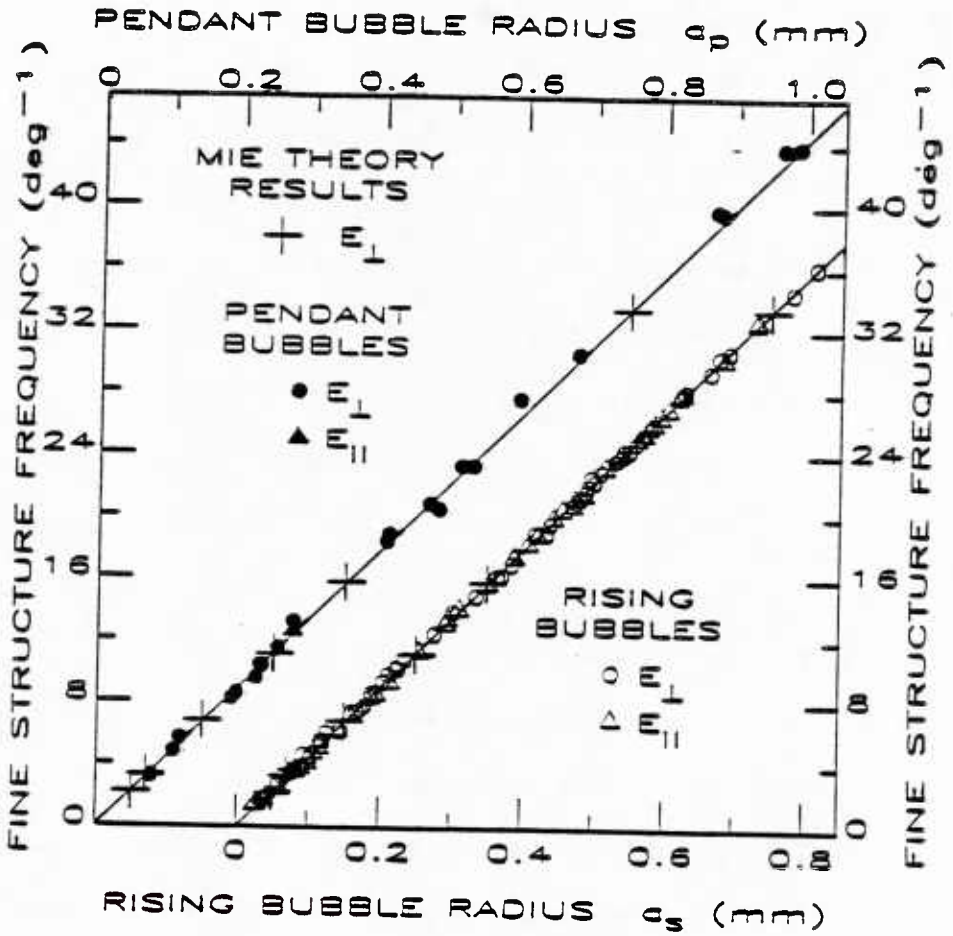

Fig. 12. Measurements and model for the angular frequency of fine-structure lines. Data are displayed for 120 rising and 23 pendant bubbles, whose radii a_s and a_p, respectively, were measured by microscope. Mie results were obtained from high-resolution computations.

they had risen through the scattering chamber. These, and other experimental details, are discussed in the Applied Optics paper.[A4]

In addition to studying the coarse structure, Langley also measured the angular spacing o the rapid oscillations evident in Fig. 9(b) which we call the "fine structure." He refined a model for the fine structure quasi-period proposed initially by Marston.[20] The results of Langley's analysis are compared with the data in Fig. 12. The comparison was carried out for a region centered on a scattering angle of 82.7 deg. The data confirms the model for both states of incident polarization (E-field parallel-to or perpendicular to the scattering plane). The smallest bubble in the rising-bubble data set had a radius of 0.026 mm while the largest bubble had a radius of 0.99 mm. The comparison also includes data for pendant bubbles which were attached to a needle. See Ref. A4 for details.

We also published a paper which shows and discussed colored bands that appear near the critical scattering angle when a bubble is illuminated with white light.[A2] For reasons of convenience the actual experiments were carried out on bubbles in glass; however, the phenomena observed should be quite similar to those present for bubbles in water. Applications to the detection and sizing of bubbles in water illuminated by white light (instead of the laser light used by Langley) are noted as are applications to the visual appearance of clouds of bubbles. A white-light bubble-size spectrometer proposed by MacIntyre[12] would make use of a related manifestation of the colored bands to measure the population spectra of microbubbles in seawater.

C. Strong cross-polarization in the near-forward scattering from bubbles: Observations of the forward optical glory.

A significant experiment was carried out which is discussed in detail in Langley's Ph.D. dissertation.[D1] This was the first observation of the

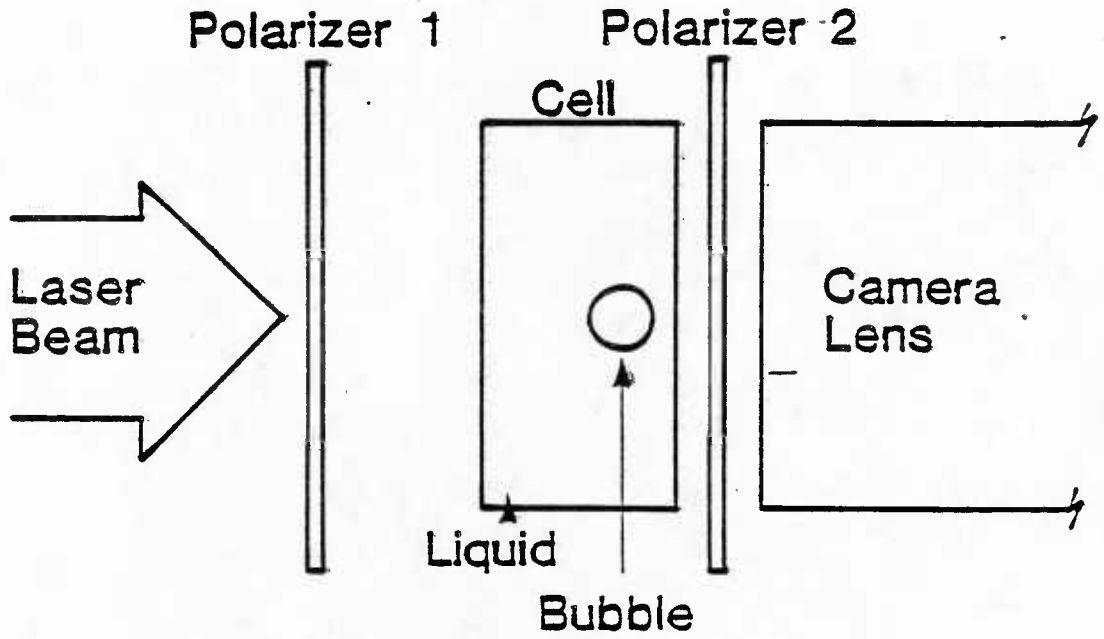

Fig. 13. Apparatus for observing forward glory scattering effects.

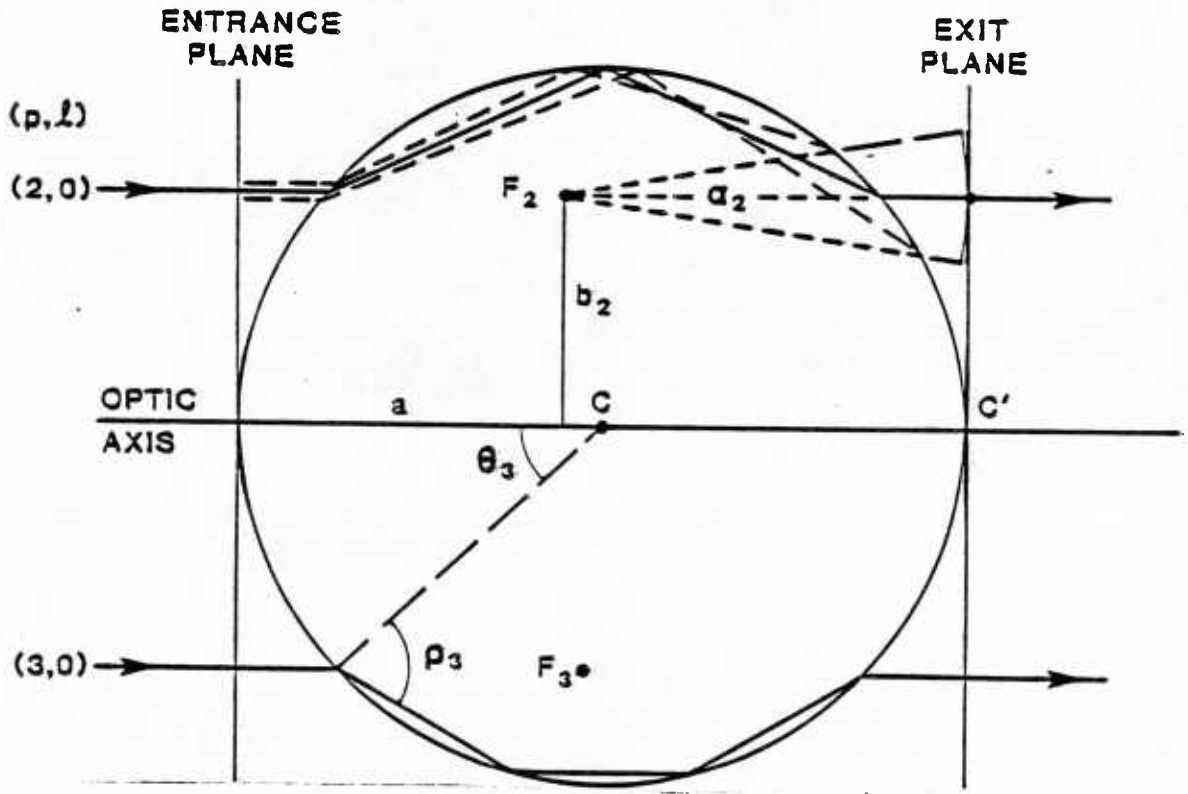

Fig. 14. Forward glory rays of a bubble and associated focal parameters. Dashed lines show the origin of the toroidal wavefront.

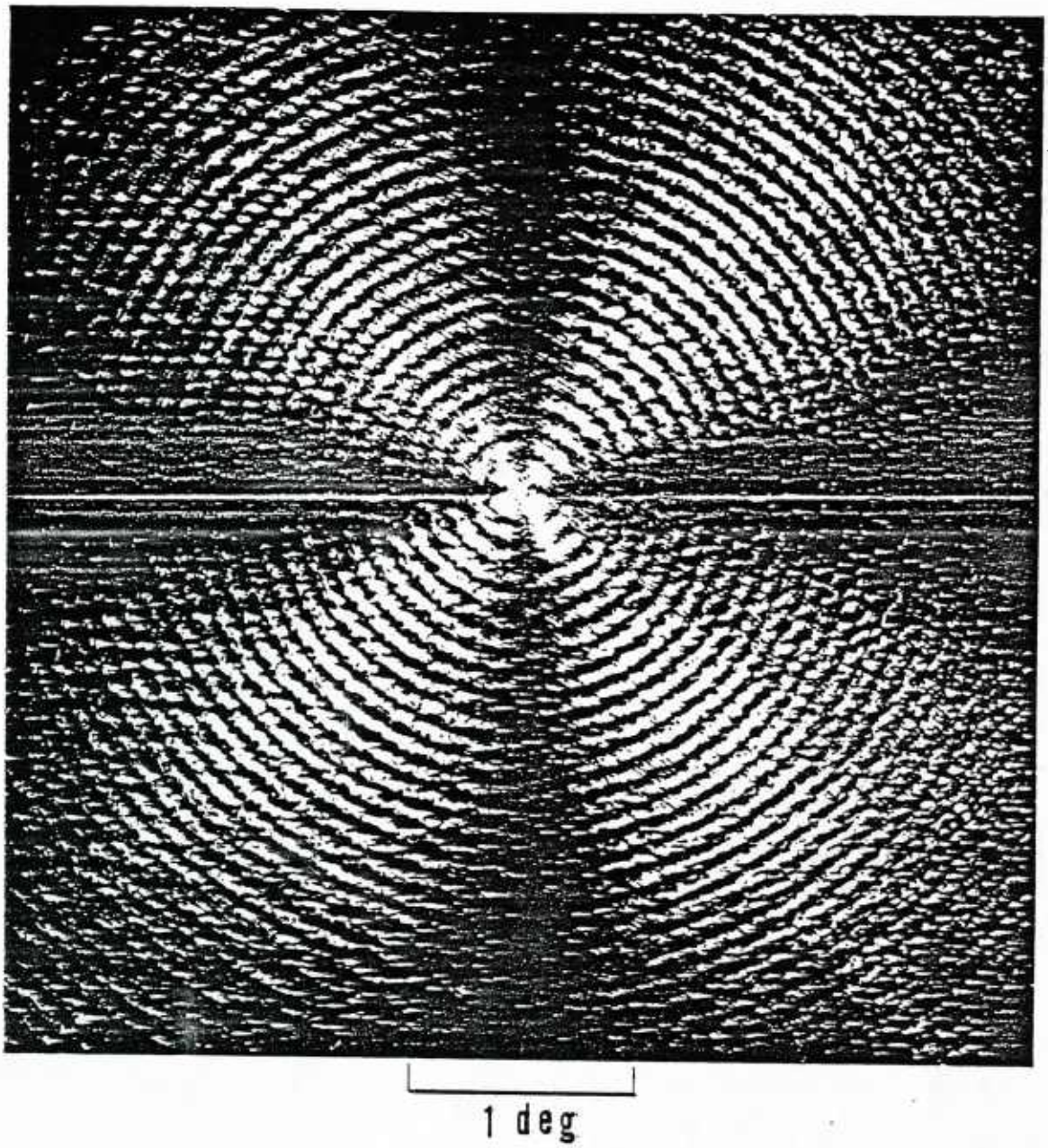

Fig. 15. Photograph of the cross-polarized near-forward scattering from a bubble of radius 0.203 mm in silicon oil.

cross-polarized forward optical glories of bubbles in water and in silicone oil. (These experiments were done in January - May of 1984 and were completed by Langley while Marston was away on a sabbatical.) A simplified diagram of the apparatus used is shown in Fig. 13. The polarizers were crossed so that in the absence of a bubble a negligible amount of light was transmitted by polarizer 2. Our theoretical analysis[20,A3,D1] shows that the principal source of near-forward cross polarized scattering should be that due to axially-focused (i.e. glory) waves. The ordinary forward-diffraction peak which contributes to the total scattering of bubbles (and also to opaque spheres or discs) is intrinsically co-polarized with the incident beam so that its contribution to the cross-polarized scattering may depend on measurement configuration.[A3] Figure 14 illustrates one class of rays producing a forward-facing axially-focused toroidal wave. (The reader may wish to compare this with Figs. 2 and 8 which illustrate rays leading to some backward facing toroidal waves.) In addition to the 2-chord wavefront shown the lower 3-chord ray also produces a toroidal wavefront. Calculations show that the dominant cross-polarized near-forward toroidal wave is the 2-chord wave for spherical bubbles either in water (refractive index = 1.33) or in silicone oil (refractive index = 1.403).

Most of the data was taken for bubbles in silicone oil. This is because the high viscosity of the oil reduces to rise velocity of bubbles so that it was easy to work with a single bubble. Calculations[D1] show that the cross-polarized irradiance from a bubble in water is similar in magnitude to that of a bubble in silicone oil and that the general angular structure of the scattering should be similar apart from small changes in scale. The far-field cross-polarized irradiance was photographed by adjusting the camera lens in Fig. 13 such that the film plane was focused at infinity. Figure 15 is a

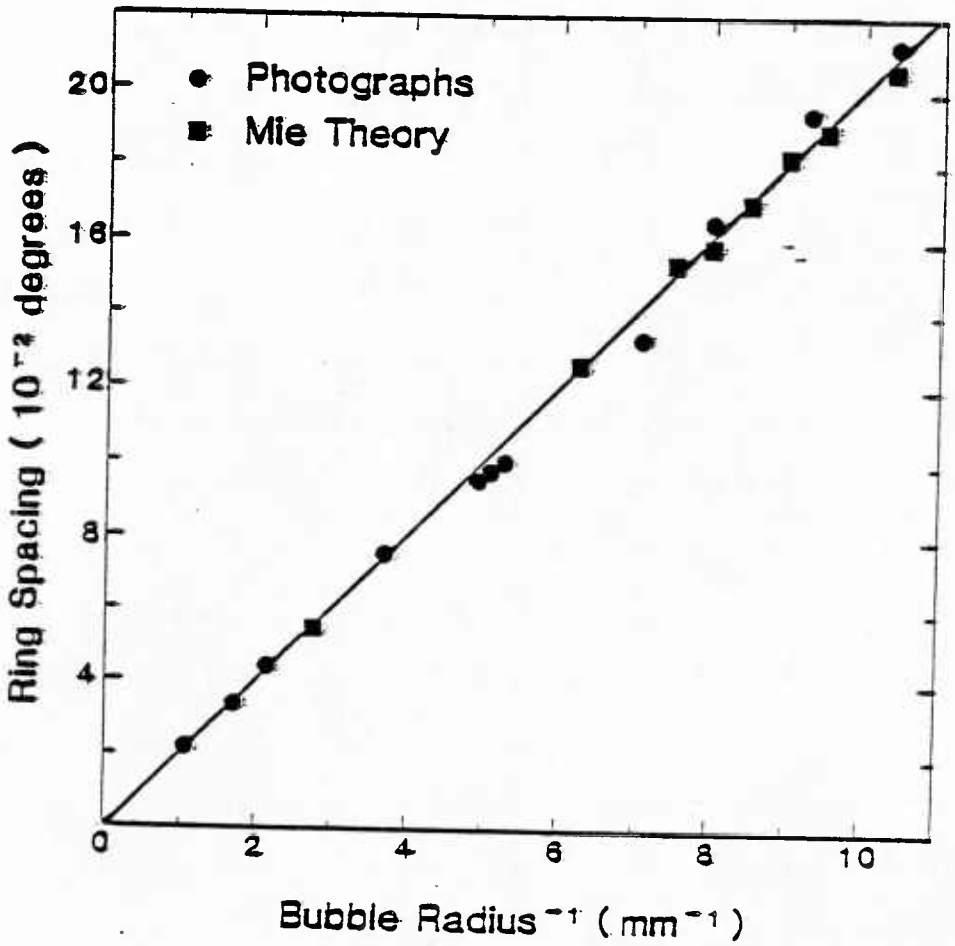

Fig. 16. Angular spacing of dark rings in the far-zone cross-polarized scattering. Measurements were made from photographs like Fig. 15 and also from Mie theory computations. The line is the physical-optics model prediction in Eq. 14.

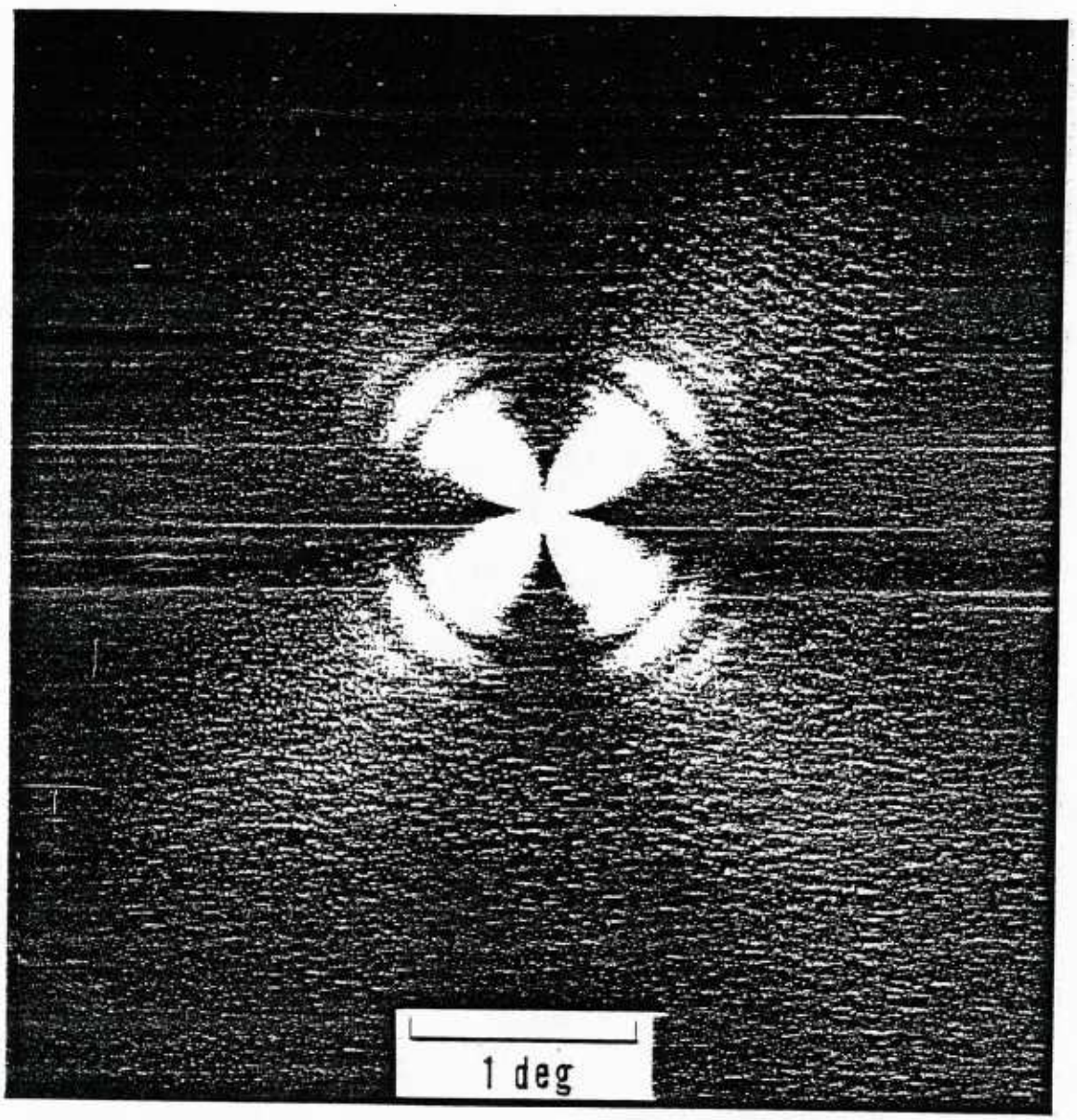

Fig. 17. Cross-polarized near-forward scattering from a cloud of small bubbles rising water.

representative photograph of the scattering for a bubble in silicone oil for a bubble whose radius a was measured to be 0.203 mm. The quasi-periodic nature of the Maltese cross-like pattern is characteristic of cross-polarized glories dominated by a single toroidal wave.[22,A9] The center of symmetry should correspond to the direction of the incident beam. Except close to the forward direction, the angular spacing of the bright (or dark) rings should be[D1]

$$\Delta\phi \simeq \frac{\pi}{ka}\left(\frac{a}{b_2}\right) \text{ radians} , \tag{14}$$

where the ratio $b_2/a = 0.65$ is independent of the bubble radius a and b_2 is the radius of the focal circle as shown in Fig. 14. Figure 16 compares the measurements with the predictions of Eq. (14). This comparison demonstrates that the cross-polarized scattering, as shown in Fig. 15, is dominated by the 2-chord toroidal wave and <u>not</u> by forward diffraction. Forward diffraction should produce angular structures having a quasi-period of

$$(\Delta\phi)_{\text{forward diffraction}} \simeq \frac{\pi}{ka} \text{ radians} , \tag{15}$$

which clearly differs from that of Eq. (14) and of the data. (Structures having a quasi-period given by Eq. (15) should, however, dominate the co-polarized scattering.)

For bubbles in water, it was not feasible to photograph the scattering from a single bubble and then to trap it. Instead the cross-polarized scattering of a cloud of small freely-rising bubbles in water was photographed. Figure 17 is a representative photograph of the scattering. For bubbles in water the quasi-period should be given by Eq. (14) with $b_2/a = 0.689$. In Fig. 17, quasi-periodic oscillations are evident with $\Delta\phi \simeq 0.005$ radian $\simeq 0.29$ deg. From Eq. (14) we estimate the average bubble

(a)

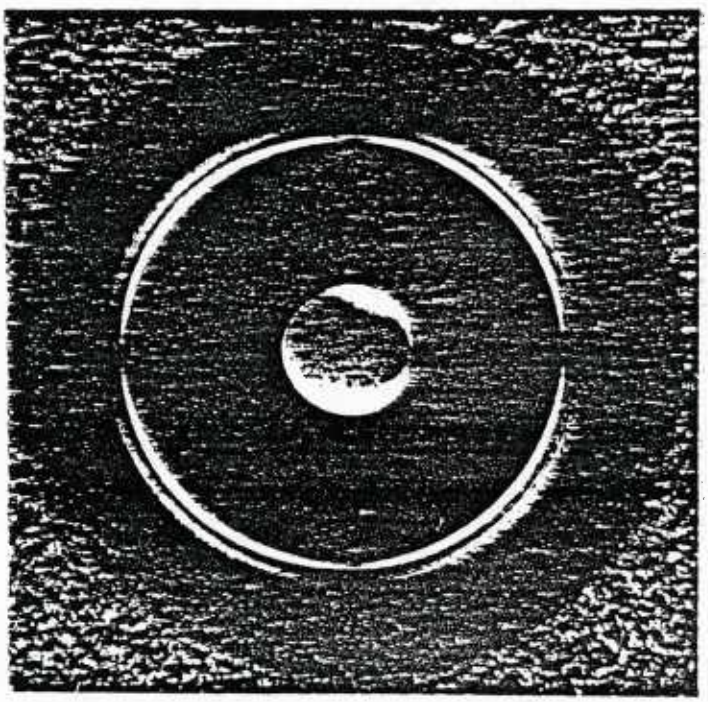

(b)

Figure 18
Photographs of the
(a) co-polarized and
(b) cross-polarized
forward glory circles
for a bubble with a
radius of 1.88 mm in
a liquid of refractive
index 1.403.

radius of the cloud to be ≃ 69 μm. These observations indicate that bubbles of this radius are sufficiently round to manifest a forward-optical glory. Bubbles in water become oblate if the radius is somewhat larger than this value so it is not known how large a bubble may be and still manifest the glory.

Cross-polarized optical glories should also be present when the incident light is circularly polarized. They should appear as in Fig. 15 and 17 except that the irradiance will not depend on the azimuthal angle so that the Maltese cross-like pattern will be lost. The pattern should be quasi-period in scattering angle. The relation between scattering patterns with linearly and circularly polarized incident light are derived by us in Ref. A9 for near backward scattering. We have also derived similar ones for near-forward scattering.

Langley also photographed[D1] the focal circles associated with the forward facing glory waves. This was done by focusing the camera in Fig. 13 directly on the bubble so that the focal circles appear as thin bright rings. The bubbles were in silicone oil. Figure 18 shows enlargements of representative photographs. In each case, more than one focal circle is visible corresponding to the sources of glory waves having different numbers of chords as in Fig. 14. The ratios of the ring radii to that of the bubble radii were measured and were found to agree with predictions.[D1]

D. Strong cross-polarization in the near-backward scattering from bubbles in water: The backward optical glory.

The principal advancements in this aspect of the research during this contract period were improvements to the theory. Observations were previously made by us (with the support of this contract) which confirmed the existence of backward glory scattering from bubbles in silicone oil[22] and in water.[A9]

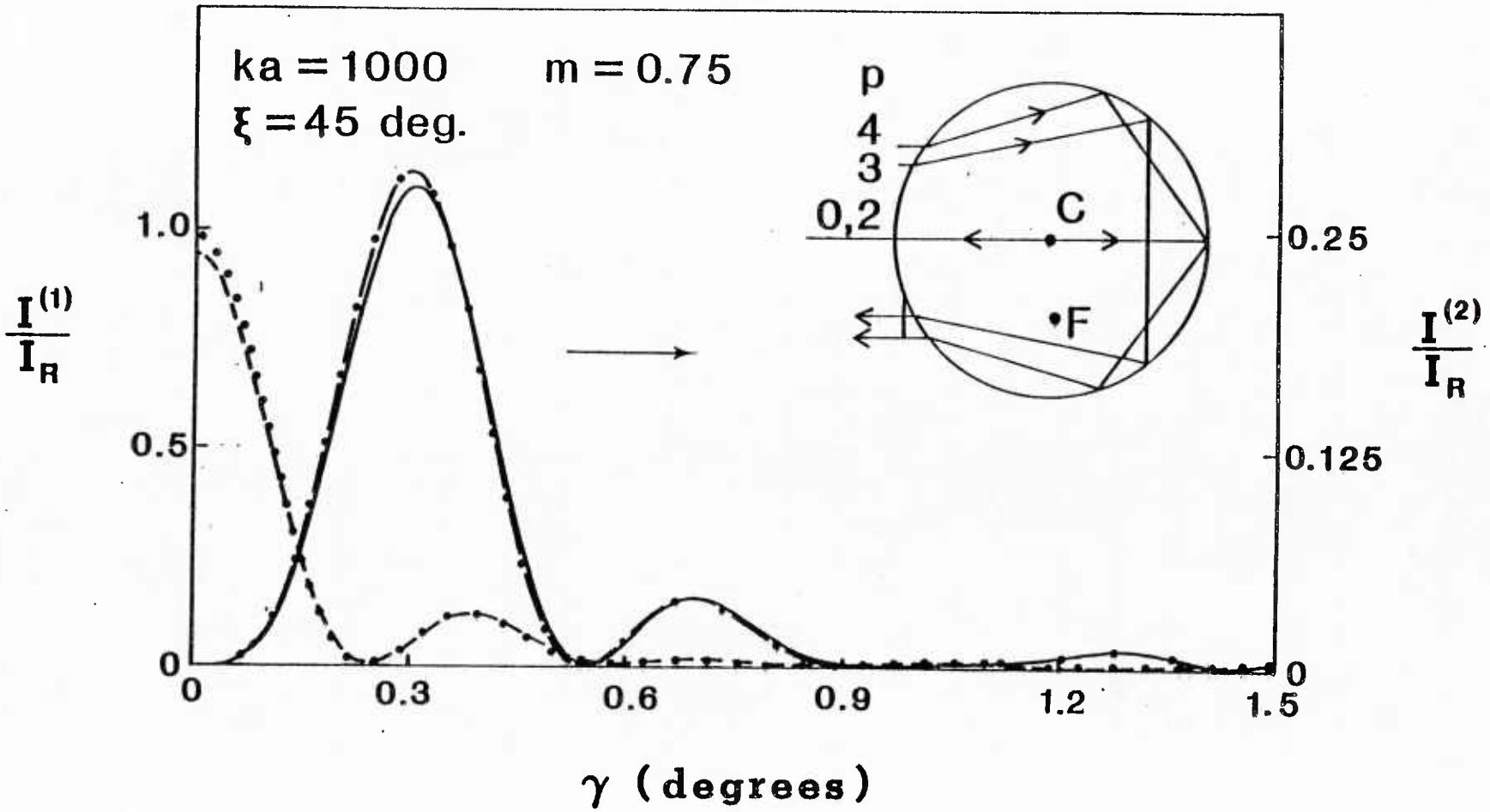

Fig. 19. Theoretical cross-polarized ($I^{(2)}$) and co-polarized ($I^{(1)}$) optical irradiances plotted as a function of the backscattering angle γ for a bubble in water of radius ≈ 66 μm (for green light). The solid and dashed curves are exact for a spherical bubble and were calculated from Mie theory. The dotted and dot-dashed curves are from a physical-optics approximation of the axially-focused (glory) waves and the specular axial reflections. Some of the rays included in the calculation are shown in the inset.

For bubbles in silicone oil the cross-polarized patterns were like that of Fig. 15.

The first theoretical advancement was to formulate a novel uniform analysis of cross-polarized and co-polarized irradiances according to Mie theory.[A3] This short paper concerns analytical details and definitions, which though important, need not be repeated here.

The other theoretical advancement is more physical in nature and merits description. For bubbles in silicone oil the cross-polarized backward glory is dominated by the 3-chord glory wave.[22] For bubbles in water, it was evident, however, that it would be necessary to sum the electric fields due to several different glory waves in order to describe the near-backward scattering. Such a summation was now possible because of the analysis of the angle-dependent phase shift of glory waves first carried out by Marston and described in the paper on the acoustic glory of fluid spheres.[1] The resulting physical-optics model predicts irradiances which agree with those given by Mie theory for spherical bubbles in water.[A9] This confirms several details of the physical-optics model of the optical glory of bubbles. Figure 19 compares Mie theory (solid and dashed curves) with model results (dotted and dot-dashed curves). The scattering is expressed in normalized units in which I_R is the irradiance which would be reflected by a perfectly reflecting sphere of the same size. The solid and dashed curves apply to cross-polarized and co-polarized irradiances and they are to be used with the right and left vertical scales, respectively. The incident light is linearly polarized and the calculation is for an aximuthal angle of 45 degrees relative to its direction of polarization. For ka = 1000, a bubble in water illuminated by green light has a radius of about 66 μm. The inset on the upper right of Fig. 19 shows some of the important rays.

E. Use of light scattering to measure the amplitude of radial oscillations of bubbles in water: An investigation of the theory.

In spite of considerable theoretical interest and practical applications, direct measurements of the response of small bubbles in water to sound of moderate or low amplitudes have not been made. Such measurements would be important since it has been recently realized that the response may be affected by the presence of surface monolayers[12] and by evaporation and condensation, both of which are difficult to model. A direct measurement would require an optical technique which was sensitive to radial pulsations with amplitudes Δa of < 2 μm. A technique with the required sensitivity was suggested by Marston in his review presentation of light scattering from bubbles given at the Workshop on Wave Propagation in Bubbly Liquids (Rosslyn, VA, May 1983) which was sponsored by the Office of Naval Research. The proposed technique, which would use features of the coarse structure in near critical-angle scattering (see Sec. IVB), is outlined below.[B8]

Stimulated in part by our descriptions[19,20,23,A4] of scattering from bubbles, G. M. Hansen and Professor L. A. Crum of the University of Mississippi recently used the coarse structure to calibrate a photometer and successfully measure the average radius of bubbles in an acoustic levitator.[29] They are also interested in direct light scattering measurements of a bubble's oscillation amplitude. Consequently the theoretical comparison of techniques outlined below is merited.

Perhaps the simplest technique for detecting small oscillations would be to scatter light at an angle close to, or equal to, the critical scattering angle of 82.7 deg. The Marston-Kingsbury approximation[23] predicts that the flux into a photometer which collects the light in a small angular region

containing this angle will be proportional to the critical-angle irradiance I_c

$$I_c \simeq \frac{1}{4} I_R \ , \quad I_R = I_{inc}(\frac{a}{2R})^2 \ , \tag{16a,b}$$

where I_R is the irradiance scattered by a perfectly reflecting sphere of the same radius a, I_{inc} is the incident irradiance, and R is the distance to the photometer from the bubble. (Corrections due to windows are assumed to be time-independent and will be neglected.) In response to a small change in a by a, the resulting shift in irradiance is due to the change in geometric cross-section. From Eq. (16) it is evidently given by

$$\Delta I_c \simeq \frac{1}{2} I_R \ (\Delta a)/a \ , \tag{17}$$

since $dI_R/da = 2\ I_R/a$.

A more sensitive (but more difficult) method of measuring a would be to place the photometer at an angle somewhat less than 82.7 deg. The observed region should be close to the center of the Nth course oscillation below 82.7 deg where the <u>slope</u> of the irradiance-versus-scattering-angle curve is predicted to be large. For example one might use 70 deg for the bubble in Fig. 9. The irradiance change will be enhanced since small changes in the radius will shift the course structure. When a increases by Δa, the coarse feature observed has an angle shift $\Delta\phi$ of approximately

$$\Delta\phi \simeq N \frac{\Omega}{2} \frac{\Delta a}{a} \ , \tag{18}$$

where we use the result[20,23] that the quasi-period Ω is roughly $\propto a^{-\frac{1}{2}}$. Let I_{pp} denote the peak-to-peak amplitude of the Nth coarse cycle. In response to the change Δa, the irradiance change ΔI is roughly

$$\Delta I \simeq 2\pi \frac{I_{pp}\Delta\phi}{2\Omega} \simeq \frac{\pi I_{pp} N\Delta a}{2a}, \qquad (19)$$

For the aforementioned example from Fig. 9 the Mie theory curve gives $I_{pp} \simeq 0.7\ I_R$ and the photometer was assumed to be set where $N = 2$. Then a comparison of Eq. (19) and (17) gives $\Delta I \simeq 4.4\ \Delta I_c$. Additional sensitivity could be achieved by placing the photometer at even smaller scattering angles since both N and I_{pp} would be larger. Furthermore, it may be argued that Eq. (19) underestimates ΔI since the increase in the geometric cross-section should give an additional term in Eq. (19) of magnitude $2\ I_R\ (\Delta a)/a$. In the final analysis, it might be necessary to calibrate the photometer using calculated Mie intensities averaged over the aperture of the photometer. It would be necessary for experimentalists to measure both the constant and the oscillating components of the photometer's output. N may be determined by counting the coarse variations in the output as the angle was varied from 82.7 deg. to the final value.

F. Rainbow-enhanced backscattering from a glass sphere in water: Theory of a novel aspect-insensitive retro-reflector for use in water.

In our paper on the acoustical glory from fluid spheres[1] a novel method for enhanced scattering was proposed which combined axial focusing with the weak focusing of rainbow or "stationary" ray. It was also noted there, that this dual focusing should enhance the light backscattered from dielectric spheres whose relative optical refractive indices were about 1.180 and 1.089. These relative indices would be realizable by placing glass spheres in water. A physical-optics model of this dual focusing, which also describes the

depolarization of the scattered electromagnetic wave, was subsequently formulated and confirmed by comparison with the results of exact Mie theory.

This research was summarized in the manuscript[A9] for the Ocean Optics VII conference. The polarization properties and (large) magnitude of the scattering illustrated by figures in that paper. Applications to the design of optical tracers, which could be made neutrally buoyant in sea water, are discussed.[A9]

G. Novel method for the discovery and classification of focused waves: Hyperbolic-umbilic diffraction catastrophe in the light scattered by an acoustically-levitated drop.

There has been recent progress in the calculation of optical[32] and acoustical[10] scattering patterns from penetrable spheroids at long wavelengths. At short wavelengths, however, partial-waves sums are difficult to evaluate and the scattering amplitudes may vary so rapidly with angle that the gross features may be difficult to identify. Furthermore, even at short wavelengths, geometric optics is not applicable near angular foci where the scattering is enhanced. This is because at foci, simple stationary phase approximations of diffraction integrals diverge.[33] Consequently, the discovery and classification of angular foci is important for the understanding of acoustical and optical short-wavelength scattering. The theoretical framework for the classification of foci was established recently (mostly by European[33] and Soviet[34] researchers) and is known as "catastrophe optics."

In a recent experiment Marston discovered a new focus or "diffraction catastrophe" in the light scattered by an acoustically levitated oblate drop of water in air.[A12,B9] A concise description of the experiment (a preprint of reference A12) is included in the present report as Sec. VIII the Appendix.

In addition to the results discussed there, the significance of this type of experiment is as follows: (i) Once the scattering patterns (Appendix, Fig. 4) were observed, it was evident that the focus must be a hyperbolic-umbilic diffraction catastrophe. It follows from previous research in catastrophe optics that no other class of focusing could explain these patterns. (ii) It is not surprising that our experiments preceded our consideration of the theory since ray tracing through (or ray reflection from) complicated shapes is difficult. It is often difficult to predict the location and types of foci in advance of a difficult calculation. Consequently, experimental searches for diffraction catastrophes in scattering patterns are worthwhile. (iii) Optical analogs may be used in place of acoustical scatterers. For penetrable objects, it is of course necessary that the optical refractive index correspond to the acoustic refractive index of interest. (iv) Once the catastrophe type has been classified, scaling laws[33] may be used to predict the scattering for other short wavelengths. For example, the intensity at the hyperbolic-umbilic focus (Fig. 4d of the Appendix) must be proportional to $(D/\lambda)^{2/3}\ (D/r)^2$ where D is the drop's diameter, λ is the wavelength, and r is the distance from the drop.

This experiment was carried out with the collaboration of Dr. E. Trinh while Marston was on a sabbatical leave (from April-June 1984) at the Jet Propulsion Laboratory (Pasadena, CA). Analysis of that data was performed by Marston after returning to Washington State University under the support of the present ONR Contract.

H. Radiation torque on a sphere caused by a circularly-polarized electromagnetic wave.

As previously noted in Sec. IVB we have calculated the scattering of circularly polarized light from bubbles.[A9] During the course of that

research, the following question was evident: "Would it be possible to use the angular momentum transport of photons (in e.g. a circularly-polarized laser beam) to spin-up a sphere?" Fundamental to this question is the calculation of the radiation torque on a sphere (of arbitrary size) caused by a circularly-polarized electromagnetic wave. This fundamental calculation had not been previously published even though there have been several investigations of the radiation pressure on spheres. Some potential applications of such a calculation include: (i) The evaluation of proposed methods for "burning" or "clearing" holes through fog with an intense laser beam. (The transport of angular momentum to drops should enhance the clearing of holes.) (ii) The estimate of instrumental bias in a proposed method for measuring fluid vorticity. (The method, based on the scattering of circularly polarized light from small spheres, may be useful in acoustics and hydrodynamics research or in remote sensing.) (iii) A novel bolometer for circularly polarized microwave radiation.

A direct calculation of the torque was carried out by Marston and Professor J. H. Crichton of Seattle Pacific University. A summary has been published[A6] and the detailed calculation has been accepted for publication in Physical Review.[A7] The simplest result is for a z-directed plane wave with pure circular polarization corresponding to a positive value of the photon spin. Formulation of the Maxwell stress dyad of the total (incident and scattered) field gives the following torque relative to the sphere's center

$$\Gamma_z = I\pi a^2 Q_{abs}/\omega .$$

Here I and ω are the incident wave's irradiance and angular frequency and a and Q_{abs} are the sphere's radius and Mie-theoretic absorption efficiency. Consequently the effective cross-section for torque is the same as that for

energy absorption $\pi a^2 Q_{abs}$. The proof is complicated since it involves detailed consideration of the angular momentum transport of multipole fields and the correction of some previous scientific literature. We have also estimated the steady-state angular velocity achieved when the torque is balanced by viscous drag[A7] and the time required to spin-up to this angular velocity.[B6]

Since the torque was found to be linked to the absorption of energy, it now appears that the effect may be too small to enhance the clearing of optical holes through fog. The absorption of radiation by the drop is more likely to be significant to the clearing process than is the torque which accompanies it; however, a detailed analysis has not been performed.

V. Characterization of Photo-Acoustic Sources

A. Production of sound by a pre-existent bubble in water illuminated by modulated light: A novel photo-acoustic source

One of the goals of this research is to examine whether pre-existent bubbles can enhance the conversion of modulated optical energy to acoustical energy. Our proposed mechanism for this energy conversion are: (i) the compression of the bubbles by optical radiation pressure and the resulting radiation of sound from the monopole oscillations of the bubble; (ii) radiation associated with monopole oscillations driven by the heating and cooling of the gas within the bubble. (The heating being due to the absorption of light by the gas and by the bubble's surface "skin" or surroundings.) We have estimated that the relevant radiation pressure is primarily due to light reflected from the bubble's surface for which the angle of incidence exceeds the critical value $\theta_c = \arcsin(n_o^{-1})$ where n_o is the liquid's refractive index. When averaged over the bubble's surface, the radial projection p_r of the radiation pressure becomes

$$p_r \simeq \frac{I}{3c}\, n_o \cos^3\theta_c \ , \qquad (20)$$

where I is the optical irradiance (watt/m^2) and c is the speed of light in a vacuum. To estimate the maximum radiated pressure, assume that the irradiance is modulated in such a way that

$$p_r = p_{r0}\,(1 + \cos \omega t) \ , \qquad (21)$$

and choose ω to correspond to the monopole resonance frequency of the bubble. The amplitude of the sound wave a distance r from a bubble of radius a is

$$p_s \simeq p_{r0}\, Q\, \frac{a}{r} \ , \qquad (22)$$

where Q is the quality factor of the resonance. For a bubble in water having $a = 20$ μm, $Q \simeq 10$ and we anticipate $|p_s| \simeq 10^{-1}$ Pa for our apparatus. This amplitude, though small, is not smaller than signals detected in conventional[35] photo-acoustic experiments. It should be emphasized that radiation due to modulated heating of the bubble may greatly exceed that predicted by (20) and (22) due to radiation pressure. The derivations of Eqs. (20) and (22) were carried out by Marston and Unger during a previous contract period. The fundamental photoacoustic mechanism proposed is different than previously known mechanisms which are reviewed in Ref 35.

To facilitate the detection of small signals radiated by single bubbles, it is necessary to "levitate" single bubbles in a quiet environment. In 1983 we demonstrated a technique for levitating bubbles by counteracting their buoyancy with the radiation force of a downward propagating laser beam. It can be shown that a stable levitation position can exist when laser is operated in the TEM^*_{01} mode which is usually described as the "doughnut" mode

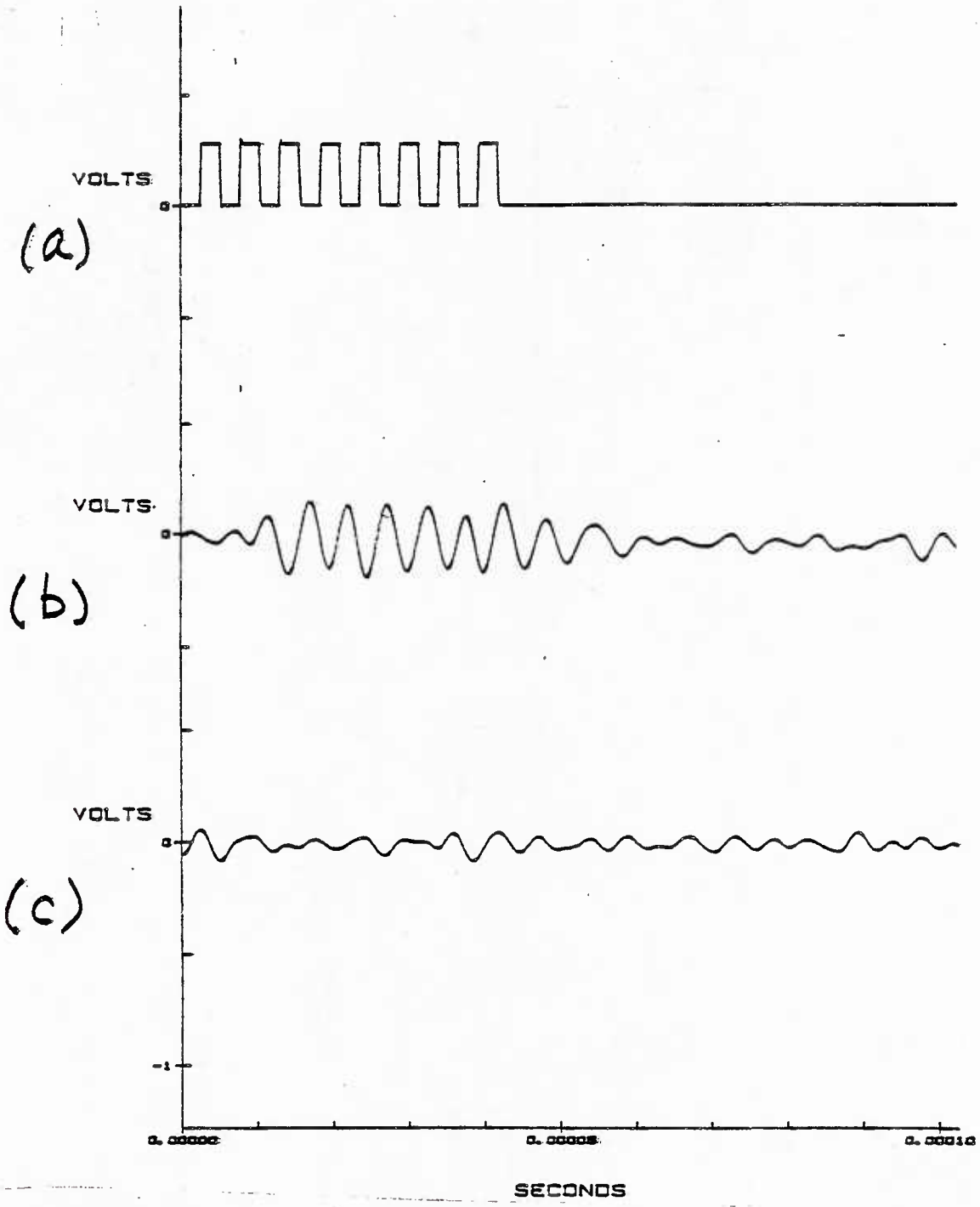

Fig. 20. Experimental evidence of the radiation of sound from a gas bubble (in water) subjected to a burst of light pulses of peak power ≃ 1 watt: (a) shows the electrical input to the optical modulator consisting of 8 equally spaced pulses each of duration ≃ 2.6 μsec; (b) shows the hydrophone signal output when a bubble is present; and (c) shows the hydrophone signal output when no bubble is present. The trace in each case is synchronized to 2.6 μsec prior to the start of the electrical input as shown in (a). Figure 21 shows the apparatus.

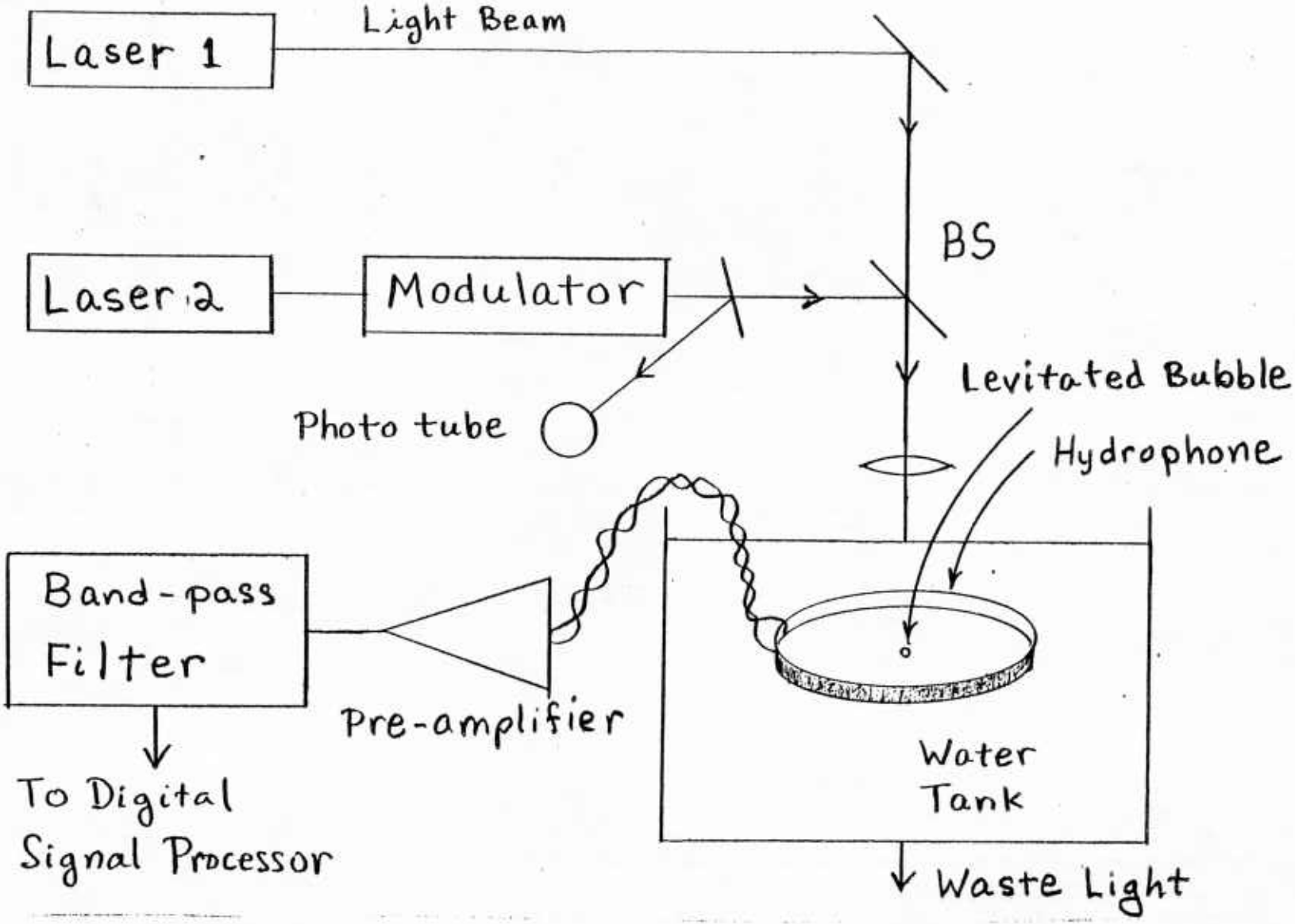

Fig. 21. Diagram of the apparatus used both to optically levitate bubbles and to subject them to bursts of light pulses. The receiver hydrophone consists of a ring of thin piezoelectric material concentric with the light beam.

because of an intensity minimum in the center of the beam. With the output of a 3 watt cw Ar-Ion laser (purchased with the combined support of contract and Washington State University funds), Unger has levitated several bubbles in the size range with radii of 10 to 25 μm for periods up to, and occasionally exceeding, 15 minutes. The bubbles contain hydrogen (H_2) gas and are generated in the water by electrolysis at the surface of a thin tungsten wire.

A simplified diagram of the apparatus for detecting the photo-acoustic response is shown in Fig. 21. The beam-splitter cube BS allows the beams from two lasers to be combined without significant power losses (because of the polarization properties of the cube and of the lasers). The combined beams are coaxial. Laser No. 1 is the aforementioned Ar-Ion laser and its beam is used to trap and levitate a single gas bubble in the water tank. Laser No. 2 is a second Ar-Ion laser made available with contract funds. Its cw beam (about 1 watt) is modulated using an electro-optic modulator system (Conoptics Model 10, Danbury, CT; purchased with contract funds). The modulated output is usually taken to be a burst of light pulses similar in form to the eight-pulse burst shown in Fig. 20(a). (Actually, Fig. 20(a) shows the electrical input to the modulator. The modulator is adjusted so that the intensity history of the burst, monitored with a photo tube is similar to the input shown.) The frequency of pulses in the burst in this case was 190 kHz. The bandwidth of the modulator is DC to 10 MHz. The reason for using a short burst is so that acoustic reflections from the surfaces of the tank would not interfere with the direct sound from the bubble. The burst was repeated 3 times per second.

Figure 20(b) shows preliminary results which appear to demonstrate a bubble acts as a photoacoustic source. It shows the output of the preamplifier averaged over 256 repetitions of the input burst shown in Fig.

20(a). That the signal in Fig. 20(b) was associated with the presence of a levitated bubble was confirmed: Fig. 20(c) shows an average obtained wit the same procedure, but immediately after the bubble had drifted out of the levitation trap. Figure 20(c) shows no signal of comparable magnitude to the one in Fig. 20(b). This is to be expected since their was negligible absorption of the green light used in this experiment. The amplitude of the sound generated by weak absorption and the usual thermal-photo-acoustic mechanism[35-37] is estimated to be small in comparison to the bubble's signal as estimated from Eq. (21). Comparison of Figs. 20(b) and 20(a) shows that signal delay is close to the expected propagation delay of about 13 μsec for travel from the bubble to the hydrophone (a distance ≃ 20 mm in water).

For technical reasons, the radius of the bubble levitated during the acquisition of Fig. 20(b) could not be measured; however, from properties of the source for this bubble, we estimate it to be about 20 μm. The monopole resonance frequency of such a bubble is about 160 kHz. The reason why the radius is not known is that the transducer blocks the direct (side) view of the bubble. Various methods for measuring the bubble's radius (with the transducer in place) are being tried, such as use of the coarse structure in the scattering discussed in Sec. IVB of this report. The data in Fig. 20(b) are representative of the two cases in which all of the subsystems (levitation, electro-optic, electro-optic modulator, and signal processing) have worked simultaneously. Attempts to obtain additional repetitions of this measurement are being carried out as of the time of this writing.

B. Transient photo-acoustic pulses generated by absorption and heating in water

The common mechanism for photo-acoustic pulse production involves transient heating and relaxation of the liquid following the bulk absorption

of a laser pulse. To be able to detect a signal by this mechanism with our apparatus (Fig. 21 with Laser 1 turned off), it was necessary to add a blue dye to the water. This is because pure water is nearly transparent to the green laser light. Our experiments typically used single pulses (of duration $\simeq$ 10 μsec) or bursts of pulses such as that shown in Fig. 20(a). They were principally carried out to confirm the magnitude of the sensitivity of our hydrophones and as a precursor to detailed hydrophone calibration experiments.

To aid in the characterization of these thermal-photoacoustic line sources, Marston examined the theory for the pressure profile radiated by a narrow light beam in a weak optical absorber.[A5] It turns out (see Ref. A5), for conditions close to those of our apparatus where the beam radius R and pulse duration Δt are such that

$$(4D\Delta t)^{1/2} < R \ll c\Delta t \ , \tag{23}$$

the pressure at distances $r \gg c\Delta t$ may be approximated by

$$p(r,t) \simeq \left(\frac{c}{8\pi r}\right)^{1/2} \left(\frac{d}{dt}\right)^{1/2} s(t - r/c) \ , \tag{24}$$

where the <u>half-order derivative operator</u> is defined in Sec. IIIF, Eq. (13a), and the instantaneous mass outflow per length-of-source $s(t)$ is

$$s(t) = \alpha\beta P(t) C_p^{-1} \ , \tag{25}$$

where $P(t)$ is the instantaneous beam power, α is the optical absorption (for which the $P \propto \exp(-\alpha z)$ where z is the propagation distance), β is the thermal coefficient of volume expansion, and C_p is the specific heat at

constant pressure. In Eqs. (23) and (24), c is the velocity of sound in water and $D \simeq 10^{-3}\,cm^2 sec^{-1}$ is the thermal diffusivity.

The evaluation of $(d/dt)^{1/2}\, s_{1/2}$, where $s_{1/2}$ is defined as in Eq. (13b), was given by Marston in Ref. A5. It would be applicable to laser pulses having $P(t) \propto s_{1/2}$; however, this is not a common time profile for a modulated laser pulse. On-the-otherhand, intensity histories from electro-optic modulators may be obtained which are well approximated by a superposition of haversine-wave bursts of the form

$$h_\infty(t) = H(\omega t)(1 - \cos\omega t) , \tag{26}$$

where H is the Heaviside unit-step function defined in Sec. IIIE and ω is radian frequency. Equation (26) represents a burst of half-infinite duration. An N cycle haversine burst is given by

$$h_N = h_\infty(t) - h_\infty\,(t - \omega^{-1}\, 2\pi N) , \tag{27}$$

for integer N. To predict the profile of such a burst, the student working on this project (Unger) has calculated that

$$(d/dt)^{1/2}\, h_\infty = \omega^{1/2}\, H(\omega t)[\sin(\omega t - \pi/4) + 2^{1/2} f(u)] , \tag{28}$$

where $u = (2\,\omega t/\pi)^{1/2}$ and f is an auxiliary Fresnel integral function defined by Eq. (7.3.5) of Abramowitz and Stegun.[38] The pressure profiles predicted for haversine bursts have smoother leading and trailing edges than the profiles of $(d/dt)^{1/2} s_N$ published in Ref. A5.

A detailed experimental confirmation of the aforementioned profile calculation has not yet been possible because of drift of the electro-optic modulator's fidelity. (This problem is judged not to be insurmountable; however, stability is important since the hydrophone's output must always be averaged over repeated bursts.) Note that other recently published

measurements[37,36] of photo-acoustic pressure profiles were for high-power laser pulses of short duration (typically less than 0.1 μsec). In those measurements, the condition $R \ll c\,\Delta t$ of Eq. (23) did not hold so that the profiles may not have been describable by Eqs. (24) and (25).

VI. Rapid Cavitation Induced by the Reflection of Shock Waves

Progress on this experiment subsequent to the publication of Ref. 39 was described in an Ad-Hoc Report issued January 6, 1984 under ONR Contract: N00014-80-C-0838. The level of support for the present contract (and our efforts to make significant progress on the research discussed in Sec. III-V of the present report) were such that there was no significant progress on this problem since the Ad-Hoc Report was issued. The principal accomplishments noted in this report are summarized below. Technical aspects are discussed in more detail in the report (which is available from P. Marston).

The research is summarized as follows:

(i) A novel technique was demonstrated for the measurement of the response of water to short duration (typically 1.7 μs) pulses of tension. The tension pulses are created by reflecting a shock (i.e. compression) pulse from a quasifree water-Mylar-air interface. The shock pulse is created when an impactor strikes a buffer plate, the water is located behind the buffer. See Fig. 22 and Ref. 39. The technical difficulties described in Ref. 39 (due to the separation of the rear Mylar surface from the water) appear to have been overcome by reducing the thickness of the rear Mylar.

(ii) The technique was used to measure dynamic tensile strengths of moderately pure (filtered and degassed) water and ethylene glycol. The majority of the water shots indicate that there was a significant amount of cavitation within 1 μs after the creation of tension (in the absence of

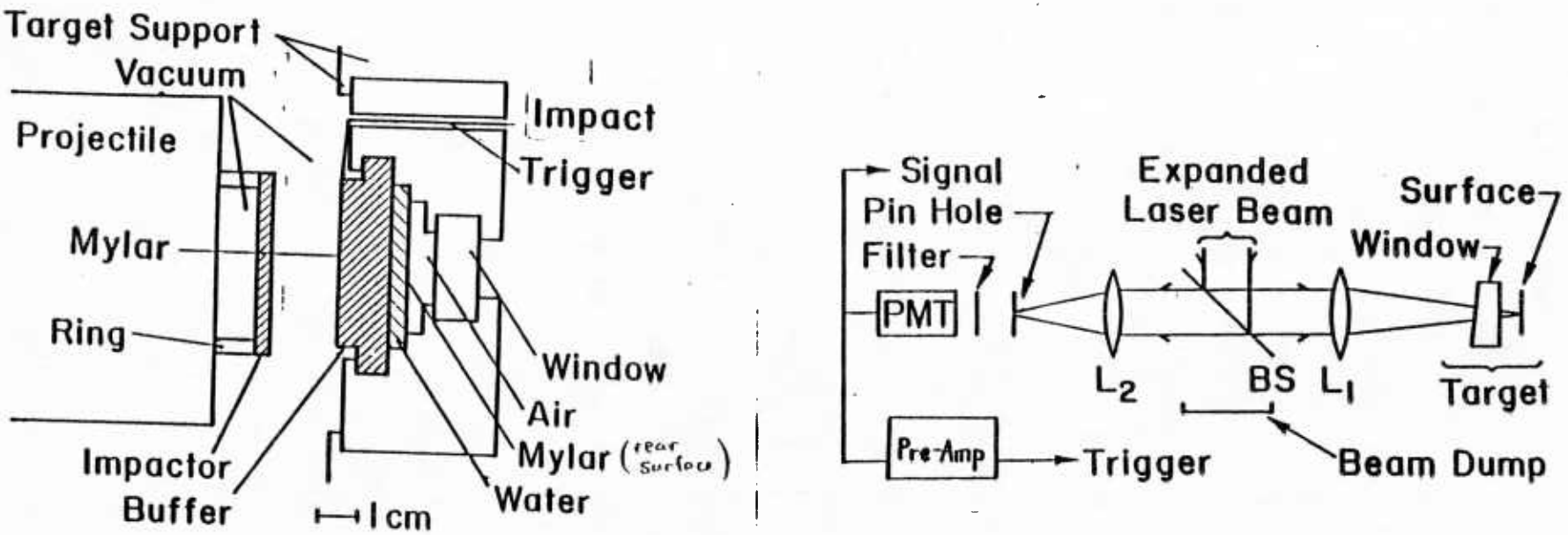

Fig. 22. Diagrams of the impactor, target, and displacement optical-interferometer used in the shock wave experiment. Rapid cavitation was induced in the water following the reflection of a shock pulse from the water-Mylar-air interface of the target.

cavitation, the negative pressures would have approached -13 MPa). The inferred dynamic tensile strength of the water was typically between 4 and 6 MPa (i.e. 40 to 60 atmospheres). Shot 4-01-82 gave a dynamic tensile strength of 11.5 MPa.

The data for ethylene glycol are more varied. The inferred dynamic tensile strengths are in excess of 4 MPa.

(iii) The impact technique developed gives meaningful results as there appears to be no other way to interpret the majority of the shot records than that given as item (ii) (above). Furthermore, there is clear evidence of reverberation of the pressure wave radiated by the bubbles within the spalled layer. The impact technique, however, is not easy to use. This is because of the low value of the impact velocity (typically 10 m/s) required for the production of compression and tension of relatively small amplitude (typically 13 MPa). By way of comparison, the typical impact experiment carried out at the Washington State University Shock Dynamics Laboratory has an impact velocity ~ 1000 m/s and a pressure ~ 2 GPa. The difficulties with <u>low-velocity</u> impact experiments are principally two-fold:

(a) A small tilt of the impactor produces a large tile of the shock and rarefaction waves. Such a tilt obscures the quantitative interpretation of the experiments. (An approximation for the increase in tilt is noted in footnote 13 of Ref. 39). To obtain meaningful experimental results, it is necessary that the tilt of the impactor be < 1 mrad $\simeq 0.06°$. This requirement necessitated the development of a novel optical alignment procedure.

(b) Reliable triggering of the oscilloscopes for the recording of data during the desired time window (which is a few s in duration) is more difficult in low-velocity shots. This difficulty was overcome

by use of two independent methods of triggering and use of several oscilloscopes (typically 5) for each shot.

To a lesser extent the following difficulties should be noted:

(c) The free-surface velocities recorded during the experiment (typically 15 m/s) are much smaller than those encountered in large-amplitude shock experiments, but larger than those in typical acoustical measurements in liquids. Consequently, a novel form of displacement interferometer was developed (described in Ref. 39) to facilitate the velocity measurements. There was occasional difficulty in aligning the interferometer and adjusting the oscilloscopes because of ambient vibrations.

(d) At the time the experiments were performed (1982), the gun facility used was a shared facility). Consequently, each shot required special adjustment of the gun and/or oscilloscopes for this particular experiment.

Technical suggestions concerning possible future experiments of this type are noted in the Ad-Hoc Report. We anticipate issuing and/or publishing a complete description of this research.

VII. References

1. P. L. Marston and D. S. Langley, "Glory and rainbow-enhanced acoustic backscattering from fluid spheres: Models of diffracted axial focusing," J. Acoust. Soc. Am. 73, 1464-1475 (1983).

2. D. L. Folds and C. D. Loggins, "Target strength of liquid-filled reflectors," J. Acoust. Soc. Am. 73, 1147-1151 (1983).

3. L. R. Dragonette, S. K. Numrich, and L. J. Frank, "Calibration technique for acoustic scattering measurements," J. Acoust. Soc. Am. 69, 1186-1189 (1981).

4. L. Flax, G. C. Gaunaurd, and H. Uberall, "Theory of resonance scattering," in Physical Acoustics XV, edited by W. P. Mason and R. N. Thurston (Academic, New York, 1981), Chap. 3, pp. 191-294.

5. G. C. Gaunaurd and H. Uberall, "RST analysis of monostatic and bistatic acoustic echoes from a elastic sphere," J. Acoust. Soc. Am. 73, 1-12 (1983).

6. G. C. Gaunaurd and A. Kalnins, "Resonances in the sonar cross sections of coated spherical shells," Int. J. Solids Structure 18, 1083-1102 (1982).

7. P. L. Marston, T. J. B. Hanson, and K. L. Williams, "Observations of the acoustic glory: scattering from an elastic sphere in near backward directions," J. Acoust. Soc. Am. suppl. 72, S106 (1982).

8. R. H. Hackman and M. F. Werby, "Nearfield effects in acoustic scattering," J. Acoust. Soc. Am. 75, 1001-1003 (1984).

9a. P. L. Marston and D. L. Kingsbury, "Acoustic scattering from fluid spheres: Diffraction and interferences near the critical scattering angle," J. Acoust. Soc. Am. 70, 1488-1495 (1981).

9b. K. Kamiuto, "Near-field scattering by a large spherical particle embedded in a nonabsorbing medium," J. Opt. Soc. Am. 73, 1819-1822 (1983).

10. R. H. Hackman, "The transition matrix for acoustic and elastic wave scattering in prolate spheroidal coordinates," J. Acoust. Soc. Am. 75, 35-45 (1984).

11. H. Medwin, "In situ acoustic measurements of microbubbles at sea," J. Geophys. Res. 82, 971-976 (1977).

12. F. MacIntyre, "On reconciling optical and acoustical bubble spectra in the mixed layer," in Proceedings of the Witecap Workshop (Galway, 4-7 Sept. 1983) in press.

13. C. F. Bohren, "Colors of the Sea," Weatherwise 36, 256-259 (1983).

14. T. C. Grenfell and D. Hedrick, "Scattering of visible and near infrared radiation by NaCl ice and glacier ice," Cold Regions Science and Technology 8, 119-127 (1983).

15. E. Silberman, "Sound velocity and attenuation in bubbly mixtures measured in standing wave tubes," J. Acoust. Soc. Am. 29, 925-933 (1957).

16. C. Gazanhes, P. Arzelies, and J. Leandre, "Propagation acoustique dans un milieu diphasique eau-bulles d'air," Acustica 55, 113-122 (1984).

17. B. R. Parkin, "Hydrodynamics and Fluid Mechanics," Naval Research Reviews XXXV, No. 4, 20-34 (1983).

18. F. A. Schraub et al., "Use of hydrogen bubbles for quantitative determination of time-dependent velocity fields in low speed water flows," J. Basic Eng. 87, 429-443 (1965).

19. D. L. Kingsbury and P. L. Marston, "Mie scattering near the critical angle of bubbles in water," J. Opt. Soc. Am. 71, 358-361 (1981).

20. P. L. Marston et al., "Light scattering by bubbles in liquids: Mie theory, physical optics approximations, and experiments," Appl. Sci. Res. 38, 373-383 (1982).

21. G. E. Davis, "Scattering of light by an air bubble in water," J. Opt. Soc. Am. 45, 572-581 (1955).

22. D. S. Langley and P. L. Marston, "Glory in optical backscattering from air bubbles," Phys. Rev. Lett. 47, 913-916 (1981).

23. P. L. Marston and D. L. Kingsbury, "Scattering by a bubble in water near the critical angle: Interference effects," J. Opt. Soc. Am. 71, 192-196 (1981); 71, 917(E) (1981).

24. A. Keller, "The influence of the cavitation nucleus spectrum on cavitation inception, investigation with a scattered-light counting method," Trans. of A.S.M.E. J. of Fluids Engineering 94, 917-925 (1972).

25. S. I. Rubinow, "Scattering from a penetrable sphere at high frequencies," Ann. Phys. (New York) 14, 305-32 (1961).

26. H. M. Nussenzveig, "High-frequency scattering by a transparent sphere: Theory of the rainbow and the glory," J. Math. Phys. 10, 125-176 (1969).

27. H. Inada and M. A. Plonus, "The geometric optics contribution to the scattering from a large dense dielectric sphere," IEEE Trans. on Antennas and Propagation AP18, 89-99 (1970.

28. F. Avellan and F. Resch, "A scattering light probe for the measurement of oceanic air bubble sizes," Int. J. Multiphase Flow 9, 649-663 (1983).

29. G. M. Hansen, "Mie-scattering as a technique for the sizing of air bubbles," Ph.D. Dissertation (Department of Physics, University of Mississippi, Oxford, MS, 1984).

30. A. J. Marker and K. H. Mader, "Light scattering from an interface bubble," Proceedings of the Society of Photo-Optical Instrumentation Engineers 362, 107-114 (1982).

31. C. D. Han (Department of Chemical Engineering, Brooklyn Polytechnic Institute) private communication, 1982.

32. S. Asano and G. Yamamoto, "Light scattering by a spheroidal particle," Applied Optics 14, 29-49 (1975); 15, 2028(E) (1976).

33. M. V. Berry and C. Upstill, "Catastrophe Optics: Morphologies of Caustics and Their Diffraction Patterns," in Progress in Optics Vol. 18, ed. E. Wolf (North-Holland, Amsterdam, 1980) pp. 257-346.

34. V. I. Arnold, Catastrophe Theory (Springer, Berlin, 1984) Chap. 8.

35. A. C. Tam, "Photoacoustics: Spectroscopy and other applications," in Ultrasensitive Laser Spectroscopy, ed. D. Kliger (Academic, New York, 1983) pp. 1-108.

36. B. Sullivan and A. C. Tam, "Profile of laser-produced acoustic pulse in a liquid," J. Acoust. Soc. Am. 75, 437-441 (1984).

37. C. Y. Kuo, M. M. F. Vieira, and C. K. N. Patel, "Transient optoacoustic pulse generation and detection," J. Appl. Phys. 55, 3333-3336 (1984).

38. M. Abramowitz and I. A. Stegun, Handbook of Mathematical Functions (Dover, N.., 1964) p. 300.

39. P. L. Marston and G. L. Pullen, "Cavitation in Water Induced by the Reflection of Shock Waves," in Shockwaves in Condensed Matter-1981, ed. by W. J. Nellis, L. Seaman, and R. A. Graham (American Institute of Physics, Proceedings No. 78, New York, 1982) pp. 515-519.

VIII. Appendix.

(A Letter submitted August 1984 to Nature)

Accepted for Publication in Nature

Rainbow scattering from spheroidal drops: a novel hyperbolic umbilic diffraction catastrophe

Philip L. Marston

Department of Physics

Washington State University

Pullman, Washington 99164 U.S.A.

Eugene H. Trinh

Jet Propulsion Laboratory

California Institute of Technology

Pasadena, California 91109 U.S.A.

(abstract)

Far-field scattering patterns were photographed for oblate spheroidal water drops illuminated by a laser beam. Near the angular region of the primary rainbow, the patterns manifest the angular dependence of a hyperbolic-umbilic (D_4^+) diffraction catastrophe where the control parameter, commonly denoted as C_3, varies with the drop's shape. Focusing corresponding to $C_3 = 0$ was observed when the drop's axis ratio $\simeq 1.3$. The scattering is novel both as rainbow phenomenology and as a manifestation of a D_4^+ diffraction catastrophe. An ultrasonic wave was used both to levitate the mm sized drops and to control their shape.

The characterization of short-wavelength scattering phenomena has been advanced by the study of diffraction catastrophes.[1,2] Examples include optical phenomena[1-5] and molecular collisions.[6] The most familiar example of a diffraction catastrophe is the ordinary rainbow.[7-9] The angular variation of the scattering from a spherical drop locally corresponds to that of a fold diffraction catastrophe,[1,2] a result most clearly seen with monochromatic illumination. Uniform approximations to rainbow scattering[8,9] have also been developed; however, these are not essential to the present research.

We studied the scattering of drops whose shape closely approximated that of an oblate spheroid with the short axis, the symmetry axis, being vertical. The drops were illuminated by a horizontally propagating gaussian beam with a wavelength $\lambda = 633$ nm. These drops were observed to scatter in the horizontal rainbow region with patterns like those of hyperbolic-umbilic (classification D_4^+) diffraction catastrophes.[1,5,6] Visible D_4^+ diffraction patterns observed previously include light transmitted by frosted glass surfaces[10] and by liquid lenses clinging to tilted glass plates.[1,4] Our observations appear to be the first report of an umbilic catastrophe associated with traditional rainbow scattering. They suggest novel phenomena to be observed in natural rainbows or in the evaluation of the partial-wave series[11] for scattering from spheroids.

The ray diagram of the primary rainbow of a spherical drop is shown in Fig. 1. For the once-reflected (twice-refracted) rays there is a minimum scattering angle of $\theta_R \simeq 138^\circ$ and the associated ray is known as the Descartes ray. When the scattering angle θ is between θ_R and 166°, there are two rays of the class shown. The rays labeled 1 and 2 are for $\theta \simeq 152^\circ$. In the two-ray region, intensity oscillations produce the supernumerary arcs.[7-9] Figure 1 is also applicable to rays which lie in the horizontal

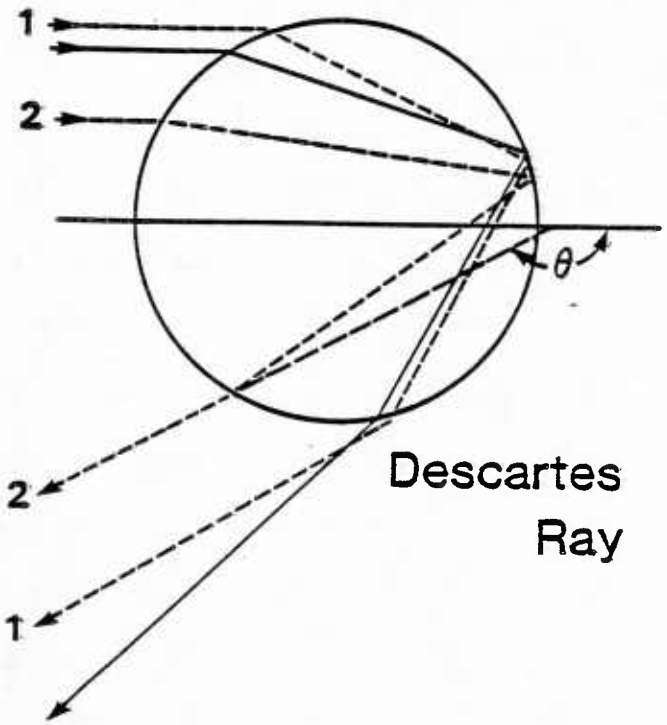

Fig. 1. Rays through either a spherical drop or through a spheroidal drop in the equatorial plane.

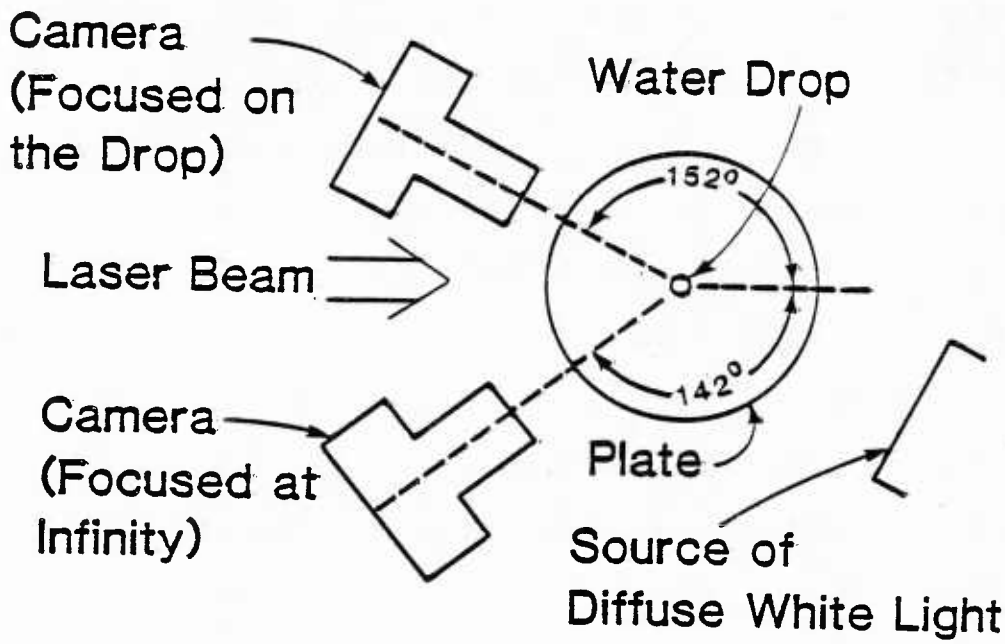

Fig. 2. Schematic view from above of the apparatus. The drop is levitated 11 mm above the plate and the optical axes of the cameras lie near a horizontal plane containing the drop. The diffuse light is usually turned off.

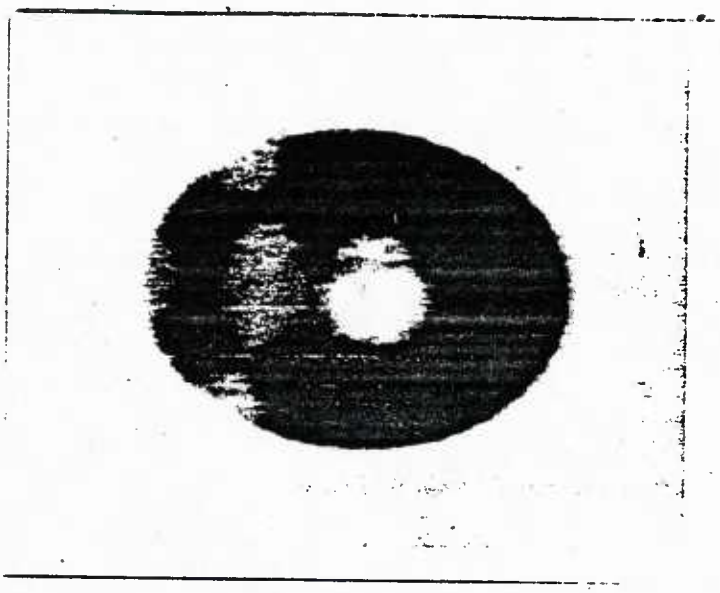

Fig. 3. Photographs of an acoustically levitated drop having a diameter D = 2.3 mm. The drop was illuminated both with diffuse light and the laser beam. The 4 bright patches on the left are due to refracted laser light.

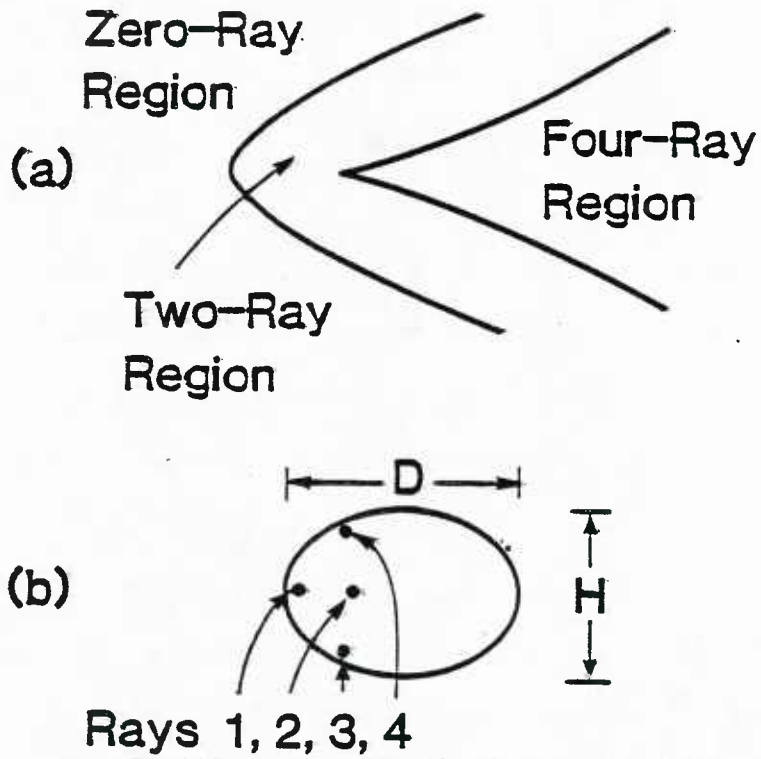

Fig. 5. (a) Partitioning of the angular regions implied by the theory of hyperbolic-umbilic diffraction catastrophes for sections having $C_3 \neq 0$. (b) Ray locations evident from the bright patches in Fig. 3. The camera's aperture was in the four-ray region.

equatorial plane P of the spheroidal drops; P cuts the drop's surface in a circle and both the incident ray and the local surface normals lie in P.

Figure 2 diagrams our apparatus. A horizontal metal plate was coupled to a piezoelectric vibrator which was driven at a frequency of 27 kHz. A curved reflector (not shown) was placed above the plate's center so as to establish an acoustic standing wave in the air below the reflector. Drops of distilled water could be levitated in this wave by an upward directed acoustic radiation pressure. The levitator is similar in principle to one described in Ref. 12. Figure 3 shows a levitated drop. The oblate shape is due to the spatial distribution of the radiation pressure.[13] In addition to the deformation evident in Fig. 3, the drop vibrates at 27 kHz with surface displacements which are too small to affect the light scattering. The drop's diameter will be denoted by D in the plane P, and by H along the vertical symmetry axis. Raising the ultrasonic amplitude increases D/H.

The scattering was photographed for randomly polarized illumination from a He-Ne laser. The camera was focused on infinity such that the pattern recorded was equivalent to that in the far field (i.e. for distances $r \gg D^2/\lambda$ from the drop). Horizontal and vertical coordinates in each photograph were linear in the horizontal and vertical scattering angles θ and β, where β is relative to the plane P. The camera viewed the region: $136^\circ < \theta < 148^\circ$, $-6^\circ < \beta < 6^\circ$.

Figure 4(a) shows the scattering from a slightly nonspherical drop having D = 1.9 mm. The intensity modulations are similar to other photographs of supernumerary arcs with laser illumination.[14] Within experimental uncertainties, their spacing is as predicted by Airy theory.[7,9] Figures 4(b)-(f) are the patterns for a different, more nonspherical, drop. For Fig. 4(b) the drop had D = 1.39 mm and D/H ≃ 1.23; somewhat smaller values of D/H gave

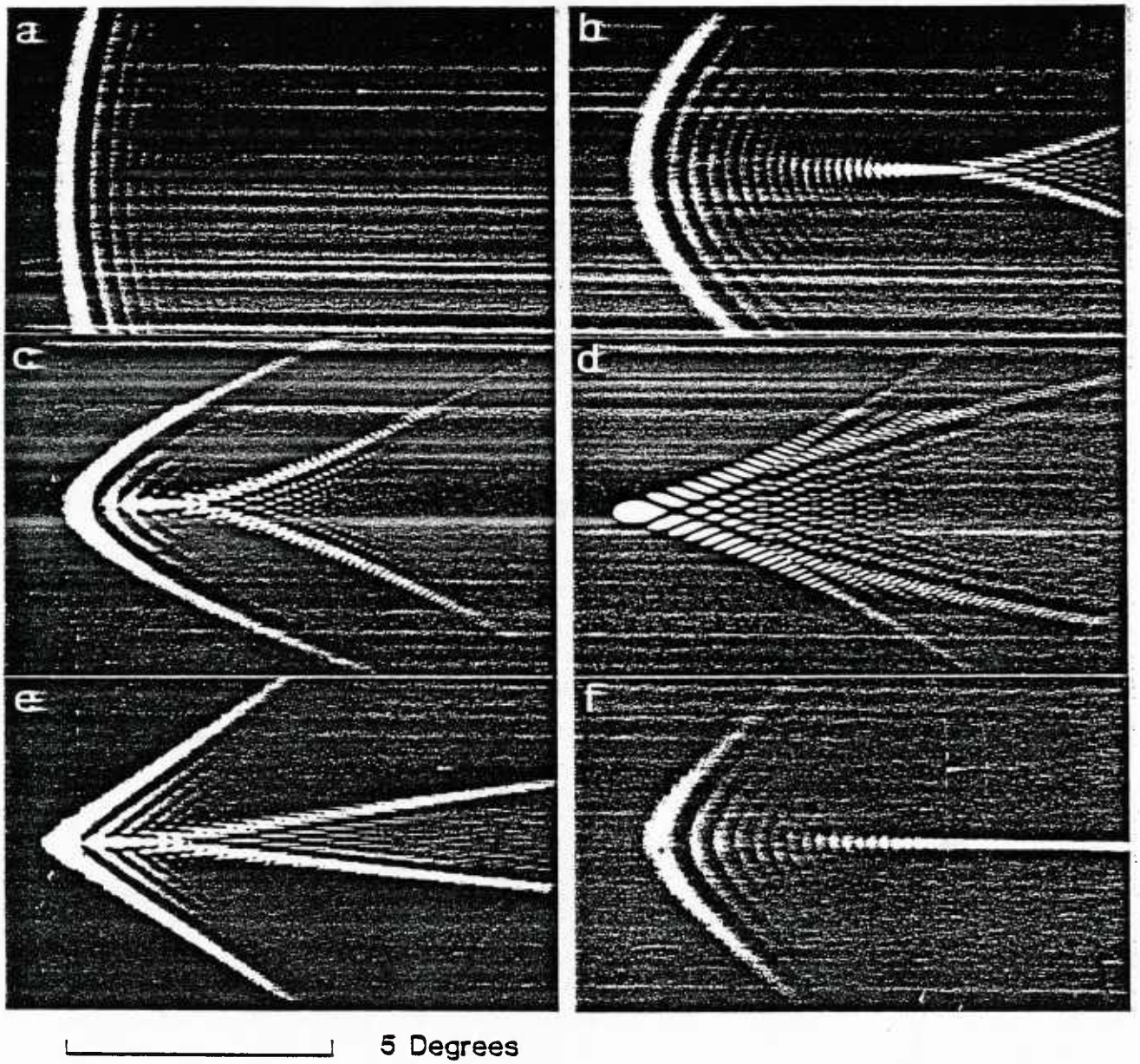

Fig. 4. Photographs of rainbow region scattering patterns arranged in order of increasing drop axis ratio D/H. The horizontal scattering angle θ increases from left to right. The cusp in (b) moved into view from the right as D/H was increased. (d) is the focal section of a hyperbolic-umbilic diffraction catastrophe while (c) and (e) manifest the unfolding of the catastrophe in response to small changes in D/H.

patterns similar to Fig. 4(a). Changes in the pattern with changes in D/H were also viewed through the camera's lens by eye.

Figure 4(d) manifests the parallelogram and caustic structures characteristic of focal section patterns of D_4^+ diffraction catastrophes. Consequently, the normal form[1,2] of the associated diffraction integral has the control parameter $C_3 = 0$. Evidently the transverse control parameters C_1 and C_2 are locally related to β and $\theta - \theta_R$ by a linear transformation. The parallelogram structure is sheared with an apex angle $\simeq 43.5 \pm 1^\circ$. Figures 4(b), (c), (e), and (f) correspond to sheared and scaled sections of D_4^+ diffraction patterns having $C_3 \neq 0$. Inspection of the patterns of the elementary catastrophes[1,4] confirms that only the D_4^+ describes our observations.

When $C_3 \neq 0$, the D_4^+ pattern may be partitioned into three angular regions according to the number of stationary points of the phase function within the diffraction integral.[1,5,6] The number of points corresponds to the number of once-reflected (twice refracted) rays which contribute to the scattering. This partitioning is illustrated in Fig. 5(a) for the pattern shown in Fig. 4(c). That the right-most region has four rays was confirmed by direct observation. A camera having a small aperture, positioned as shown in Fig. 2, was focused on the drop. Figure 5(b) is drawn from a representative image so as to show the locations of the four observed rays. Rays 1 and 2 lie in the plane P and correspond to those in Fig. 1. Rays 3 and 4 are horizontally directed, having $\beta \simeq 0^\circ$ when outside the drop. They are skew rays since <u>inside</u> the drop they do not lie in a horizontal plane. These rays were not anticipated from previous studies[14,15] of rainbows of spheroidal drops which considered only rays confined to a plane.

Other features observed were consistent with those expected of a D_4^+ diffraction catastrophe at short wavelengths $\lambda \ll D$. The axis ratio D/H

which gives $C_3 = 0$ should be independent of D for spheroidal drops having the same refractive index. To check this prediction, drops were illuminated with diffuse white light (see Fig. 2) and their profiles were photographed. Prior to each photograph, D/H was adjusted so that the laser scattering pattern was a focal section as in Fig. 4(d). Photographs of six drops having D of 1.5 to 2.4 mm gave axis ratios not correlated with D. The average measured D/H of 1.305 ± 0.016 is a lower limit of the true axis ratio since any misalignment of the camera's optical axis from the equatorial plane would give a systematic reduction in the measured D/H.

For scattering from large spherical drops, Airy's theory[1,7] predicts that when $\theta = \theta_R$, the intensity I at a distance r has $I \propto (D/\lambda)^{1/3}(D/r)^2$. Examination of the D_4^+ diffraction integral[1,5,6] gives $I \propto (D/\lambda)^{2/3}(D/r)^2$ when C_3, β, and $\theta - \theta_R$ all vanish. Visual inspections and photographs confirm that the scattering near the apex of the focal section appears brighter than that near θ_R of the other sections such as Fig. 4(b) and (c). This focusing for $C_3 \simeq 0$ may be observable in nature when the sun is close to the horizon. Raindrops having $D \simeq 4$ mm have an axis ratio $\simeq 1.3$. However, such large drops are flattened below the waistline[16] and the effect on the focusing is not known.

These experiments were carried out while P. Marston was at Jet Propulsion Laboratory on a sabbatical leave. The research was partially supported by the U.S. National Aeronautics and Space Administration and by the Office of Naval Research.

References

1. Berry, M. V. and Upstill, C. in Progress in Optics Vol. 18 (ed. Wolf, E.) 257-346 (North-Holland, Amsterdam, 1980).
2. Berry, M. V. in Physics of Defects (eds. Balian, R., Kléman, M. and Poirier J.-P.) 453-543 (North-Holland, Amsterdam, 1981).
3. Berry, M. V. and Nye, J. F. Nature 267, 34-36 (1977).
4. Nye, J. F. Phil. Trans. R. Soc. A 292, 25-44 (1979).
5. Gilmore, R. Catastrophe Theory for Scientists and Engineers (Wiley, New York, 1981).
6. Uzer, T., Muckerman, J. T. and Child, J. T. Molec. Phys. 50, 1214-1230 (1983).
7. Van de Hulst, H. C. Light Scattering by Small Particles (Wiley, New York, 1957).
8. Khare, V. and Nuzzenzveig, H. M. Phys. Rev. Lett. 33, 976-980 (1974).
9. Konnen, G. P. and deBoer, J. H. Appl. Opt. 18, 1961-1965 (1979).
10. Berry M. V. J. Phys. A: Gen. Phys. 8, 566-583 (1975).
11. Asano, S. and Yamamoto, G. Appl. Opt. 14, 29-49 (1975).
12. Hanson, A. R., Domich, E. G. and Adams, H. S. Rev. Sci. Instrum. 35, 1031-1034 (1964).
13. Marston, P. L., LoPorto-Arione, S. E. and Pullen, G. L. J. Acoust. Soc. Am. 69, 1499-1501 (1981); Errata ibid 71, 511-512 (1982).
14. Marston, P. L. Appl. Opt. 19, 680-685 (1980).
15. Fraser, A. B. J. Opt. Soc. Am. 73, 1626-1628 (1983).
16. Green, A. W. J. Appl. Meteorol. 14, 1578-1583 (1975).

APRIL 1984

REPORTS DISTRIBUTION LIST FOR ONR PHYSICS DIVISION OFFICE
UNCLASSIFIED CONTRACTS

Director
Defense Advanced Research Projects Agency
Attn: Technical Library
1400 Wilson Blvd.
Arlington, Virginia 22209
1 copy

Office of Naval Research
Physics Division Office (Code 412)
800 North Quincy Street
Arlington, Virginia 22217
2 copies

Office of Naval Research
Director, Technology (Code 200)
800 North Quincy Street
Arlington, Virginia 22217
1 copy

Naval Research Laboratory
Department of the Navy
Attn: Technical Library
Washington, DC 20375
1 copy

Office of the Director of Defense
Research and Engineering
Information Office Library Branch
The Pentagon
Washington, DC 20301
1 copy

U.S. Army Research Office
Box 1211
Research Triangle Park
North Carolina 27709
2 copies

Defense Technical Information Center
Cameron Station
Alexandria, Virginia 22314
12 copies

Director, National Bureau of Standards
Attn: Technical Library
Washington, DC 20234
1 copy

Director
U.S. Army Engineering Research
and Development Laboratories
Attn: Technical Documents Center
Fort Belvoir, Virginia 22060
1 copy

ODDR&E Advisory Group on Electron Devices
201 Varick Street
New York, New York 10014
1 copy

Air Force Office of Scientific Research
Department of the Air Force
Bolling AFB, DC 22209
1 copy

Air Force Weapons Laboratory
Technical Library
Kirtland Air Force Base
Albuquerque, New Mexico 87117
1 copy

Air Force Avionics Laboratory
Air Force Systems Command
Technical Library
Wright-Patterson Air Force Base
Dayton, Ohio 45433
1 copy

Lawrence Livermore Laboratory
Attn: Dr. W. F. Krupke
University of California
P.O. Box 808
Livermore, California 94550
1 copy

Harry Diamond Laboratories
Technical Library
2800 Powder Mill Road
Adelphi, Maryland 20783
1 copy

Naval Air Development Center
Attn: Technical Library
Johnsville
Warminster, Pennsylvania 18974
1 copy

Naval Weapons Center
Technical Library (Code 753)
China Lake, California 93555
1 copy

Naval Underwater Systems Center
Technical Center
New London, Connecticut 06320
1 copy

Commandant of the Marine Corps
Scientific Advisor (Code RD-1)
Washington, DC 20380
1 copy

Naval Ordnance Station
Technical Library
Indian Head, Maryland 20640
1 copy

Naval Postgraduate School
Technical Library (Code 0212)
Monterey, California 93940
1 copy

Naval Missile Center
Technical Library (Code 5632.2)
Point Mugu, California 93010
1 copy

Naval Ordnance Station
Technical Library
Louisville, Kentucky 40214
1 copy

Commanding Officer
Naval Ocean Research & Development Activity
Technical Library
NSTL Station, Mississippi 39529
1 copy

Naval Explosive Ordnance Disposal Facility
Technical Library
Indian Head, Maryland 20640
1 copy

Naval Ocean Systems Center
Technical Library
San Diego, California 92152
1 copy

Naval Surface Weapons Center
Technical Library
Silver Spring, Maryland 20910
1 copy

Naval Ship Research and Development Center
Central Library (Code L42 and L43)
Bethesda, Maryland 20084
1 copy

Naval Avionics Facility
Technical Library
Indianapolis, Indiana 46218
1 copy